/
Article / Book Information

( )	
Title(English)	Nonmesonic weak decays of light hypernuclei
( )	
Author(English)	Inoue Takashi
( )	: ( ), : , : 3382 , :1997 3 26 , : , :
Citation(English)	Degree:Doctor (Science), Conferring organization: Tokyo Institute of Technology, Report number: 3382 , Conferred date:1997/3/26, Degree Type:Course doctor, Examiner:
( )	
Type(English)	Doctoral Thesis

Nonmesonic Weak Decays of Light Hypernuclei

Takashi Inoue

Department of Physics, Tokyo Institute of Technology

Meguro, Tokyo 152, Japan

Abstract

The nonmesonic decays of hypernuclei are studied. The $\Lambda N \to NN$ transition has described not only by the one pion exchange mechanism but also by a new mechanism, which correspond to the quark degrees of freedom in the two baryons. By employing a realistic wave function of the decaying Λ inside the hypernuclei, nonmesonic decay rates of $^4_\Lambda H$, $^4_\Lambda He$, and $^5_\Lambda He$ are obtained. The result shows that the new direct quark mechanism is significant and essential to understand some features of the nonmesonic decays of light hypernuclei. Furthermore, we have found that the direct quark mechanism has a large $\Delta I = 3/2$ contribution in the $J = 0$ channel.

2

Contents

4

Chapter 1

Introduction

1.1 Weak decays of hypernuclei

A baryon which has strangeness, such as Λ and Σ, is called hyperon, and a nucleus which contains a hyperon or hyperons is called hypernucleus. Generally, the hyperon is stable against strong interaction which conserves strangeness, but it decays via weak interaction which changes the flavor. Therefore hypernuclei in their ground states also decay via a weak interaction when they are stable against strong decay mode such as particle emission. This is called the weak decay of hypernuclei. Because only the Λ hypernuclei are studied in this paper, we simply call Λ-hypernuclei hypernuclei.

A free Λ hyperon mostly decays into a nucleon and a pion

$$\Lambda \;\rightarrow\; p + \pi^- + 37.8\text{MeV} \quad 64\% \tag{1.1}$$

$$\rightarrow\; n + \pi^0 + 41.1\text{MeV} \quad 36\% \tag{1.2}$$

and its life time is $t_\Lambda = \hbar/\Gamma_\Lambda = 2.63 \times 10^{-10}$ sec [1]. These are a typical nonleptonic weak processes. The change of the isospin, ΔI, in this decay is equal to 1/2 or 3/2 because the Λ hyperon has isospin 0, the nucleon has isospin 1/2 and the pion has isospin 1. The Clebsch-Gordan coefficient for the isospin sum tells us that if ΔI is equal to 1/2 the ratio $p\pi^-$ to $n\pi^0$ becomes 2:1. The experimental data are close to 2:1 and indicate that the $\Delta I = 1/2$ part is dominant in the decay. This feature is seen widely in the nonleptonic weak decays of strange hadrons and called the $\Delta I = 1/2$ rule [2]. This phenomenological selection rule is not naively

resulted from the standard theory of weak electro-magnetic interaction, the Weinberg-Salam theory, which is the fundamental theory of the weak electro-magnetic interaction. In fact, in the decay of strange quark with exchange of one W boson, $\Delta I = 3/2$ takes place as strongly as $\Delta I = 1/2$. Therefore the empirical $\Delta I = 1/2$ dominance is considered due to the effects of the strong interaction between quarks in decay process. It is known that a part of the strong interaction corrections can be estimated by using the renormalization group improved perturbation theory of QCD [2, 3, 4, 5], while the effects of low-energy nonpertubative hadronic interactions is not quantitatively understood.

A weak decay of hypernuclei is a weak decay of hyperon in many body systems. The situation is very different form the free decay. There are two different decay modes. One is the decay which emits a pion and is called the π-mesonic decay. Another is the decay which does not emits pion and is called the nonmesonic decay. The microscopic process of the mesonic decay is $\Lambda \to N\pi$, which is the same as the free Λ decay. While the microscopic process of nonmesonic decay is considered to be the two-body $\Lambda N \to NN$ weak process.

$$\Lambda + p \to n + p + 176\text{MeV} \tag{1.3}$$

$$\Lambda + n \to n + n + 176\text{MeV} . \tag{1.4}$$

The nonmesonic decay is a significant decay. In fact its rate is about a half of total decay for light hypernuclei, and becomes dominant in heavy hypernuclei [6, 7, 8, 9, 10, 11, 12]. We can understand this feature as follows. Because the $\Lambda \to N\pi$ transition produces the final nucleon with a low momentum, the mesonic decay is suppressed by the Pauli exclusion principle inside nuclei. On the other hand, because the $\Lambda N \to NN$ transition produces the final nucleons with large momenta, the effect of Pauli exclusion principle becomes small. The final nucleon has a momentum of approximately 400 MeV/c, which is much larger than the nulear Fermi momentum $k_F \simeq 280$ MeV/c.

The $\Lambda N \to NN$ process is very interesting. It is a new type of non-leptonic weak process. It may be useful to look into this process, in order to study the effect of strong interaction to the nonleptonic weak processes. And it might expose the substructure of baryon due to its large momentum transfer. For example, how the quark structure affects this process, the relation to the parity violating nuclear force which is another two baryon weak process

6

and whether the phenomenological $\Delta I = 1/2$ rule holds or not are some of the interesting subjects.

The theoretical study of $\Lambda N \rightarrow NN$ has traditionally based on the meson exchange picture. There the meson-baryon-baryon weak vertex is determined phenomenologically so as to describe the free hyperon decays, and therefore satisfies the $\Delta I = 1/2$ rule automatically. Recent experimental data, however, have revealed some difficulties in the meson exchange picture. For instance, the predicted n-p ratio is much smaller than the experimental data for light hypernuclei.

These days, hypernuclei are observed in the counter experiment of such as the (K^-, π^-) strangeness exchange reaction, and its structure and decay phenomena are studied. At present, such experiments are carried out at KEK in Tukuba and the Brookhaven National Laboratory(BNL) in USA. At KEK, the secondary beams of π and K mesons are produced by colliding the 12 GeV proton beam from the proton synchrotron to a target. Then hyperons and hypernuclei with strangeness -1 or -2 are produced. In the BNL, the AGS synchrotron is used.

The project so called the Japan Hadron Project(JHP) is carried forward by leadership of INS of University of Tokyo. In the project, the 50 GeV high intensity proton synchrotron will be constructed. When the accelerator is operated, production of more than hundred times hypernuclei compared to 12 GeV proton synchrotron is expected. The hypernuclear study will be developed very much.

In this thesis we study the nonmesonic weak decays of light hypernuclei theoretically. We emphasize the quark substructure of the Λ and N baryons in the process. We propose a new direct quark (DQ) mechanism for the $\Lambda N \rightarrow NN$ transition, which is induced by the direct quark-quark weak transition expected in the standard electro-weak theory. We construct the transition potential induced by the DQ mechanism and incorporate it in evaluating the nonmesonic decays of light hypernuclei. We show that the new mechanism is significant and essential to understand some features of the nonmesonic decays of hypernuclei.

This thesis is organized as follows. In the rest of this chapter, we briefly study the weak interaction of quarks, constituent quark picture of hadron and hyperon-nucleon force in a nuclei. In chapter 2, he weak $\Lambda N \rightarrow NN$ transition is studied. We propose the DQ

7

mechanism and calculate the corresponding potential. In chapter 3, we study the nonmesonic decay of the light s-shell hypernuclei: $^4_\Lambda$H, $^4_\Lambda$He, and $^5_\Lambda$He. The decay rates are calculated with realistic wave functions of the decaying Λ inside the hypernuclei. Chapter 4 is devoted to the summary.

1.2 Weak interaction of hadron in the standard theory

In this section, we study the weak interaction of hadron.

The standard theory of weak electro-magnetic interaction which is so called Weinberg-Salam theory, gives the weak interaction of quarks. Therefore the weak interaction of hadron is also given because hadron are made of quarks. But it is not easy to evaluate the weak interaction of hadron since quarks are always influenced by the strong interaction. In the case of non-leptonic processes, we need the weak interaction between two quarks. One can easily expect that effects of strong interaction are especially important in these interaction. In the following, we briefly study this interaction in the strangeness changing case. The Hamiltonian for this interaction has been calculated by several authors [2, 3, 4, 5]. We review along the work of Gilman and Wise and the work of Paschos, Schneider and Wu.

In the standard theory, strangeness changing weak interaction of quarks is described by the vertex

$$H_W(x) = \frac{g_W}{2\sqrt{2}} J_\mu^+(x) W_\mu^-(x) + H.c. , \tag{1.5}$$

where W_μ^- is the charged-W-boson field and J_μ^+ is the hadronic charged weak current. The weak currents are composed of left handed fermion. Therefor, for example, it is given by

$$
\begin{aligned}
J_\mu^+(x) &= \bar{u}_\alpha(x)\gamma_\mu(1-\gamma_5)d'_\alpha(x) + \bar{c}_\alpha(x)\gamma_\mu(1-\gamma_5)s'_\alpha(x) + \bar{t}_\alpha(x)\gamma_\mu(1-\gamma_5)b'_\alpha(x) \\
&= (\bar{u}_\alpha d'_\alpha)_{V-A} + (\bar{c}_\alpha s'_\alpha)_{V-A} + (\bar{t}_\alpha b'_\alpha)_{V-A} .
\end{aligned} \tag{1.6}
$$

where α denotes the color of quarks and the color sum is always assumed. Note that the standard theory contains no flavor changing neutral current.

One can define the effective Hamiltonian $H_{eff}^{\Delta S=1}$ by

$$\langle| H_{eff}^{\Delta S=1} |\rangle = -\frac{i}{2} \int d^4x \langle| T H_W(x) H_W(0) |\rangle \tag{1.7}$$

where RHS is the nonleptonic weak transition matrix element between low-momentum hadron states differing in strangeness by one. In real world, such processes have a energy scale of several hundred MeV and the effective Hamiltonian $H_{eff}^{\Delta S=1}$ could be written in terms of the light u, d and s quark fields.

If the process has the energy scale larger than bottom quark mass but smaller than the W boson mass, the effective Hamiltonian $H_{eff}^{\Delta S=1}$ can be written in terms of the u, d, s, c and b quark fields. Therefore it can be expanded as

$$H_{eff} = -\frac{G_f}{2\sqrt{2}} \left\{ \xi_c A^{c(+)}\left(\frac{m_W}{\mu},g\right) O_c^+ + \xi_c A^{c(-)}\left(\frac{m_W}{\mu},g\right) O_c^- + \xi_t \sum_{r=1}^{6} A_r^t\left(\frac{m_W}{\mu},g\right) O_r \right\} \quad (1.8)$$

where the local oparators are defined by

$$O_c^\pm = \left[(\bar{s}u)_{V-A}(\bar{u}d)_{V-A} \pm (\bar{s}u)_{V-A}(\bar{u}u)_{V-A}\right] - (u \to c) \qquad (1.9)$$

$$O_1 = (\bar{s}_\alpha d_\alpha)_{V-A}(\bar{u}_\beta u_\beta)_{V-A} \qquad (1.10)$$

$$O_2 = (\bar{s}_\alpha d_\beta)_{V-A}(\bar{u}_\beta u_\alpha)_{V-A} \qquad (1.11)$$

$$O_3 = (\bar{s}_\alpha d_\alpha)_{V-A}\left[(\bar{u}_\beta u_\beta)_{V-A} + \cdots + (\bar{b}_\beta b_\beta)_{V-A}\right] \qquad (1.12)$$

$$O_4 = (\bar{s}_\alpha d_\beta)_{V-A}\left[(\bar{u}_\beta u_\alpha)_{V-A} + \cdots + (\bar{b}_\beta b_\alpha)_{V-A}\right] \qquad (1.13)$$

$$O_5 = (\bar{s}_\alpha d_\alpha)_{V-A}\left[(\bar{u}_\beta u_\beta)_{V+A} + \cdots + (\bar{b}_\beta b_\beta)_{V+A}\right] \qquad (1.14)$$

$$O_6 = (\bar{s}_\alpha d_\beta)_{V-A}\left[(\bar{u}_\beta u_\alpha)_{V+A} + \cdots + (\bar{b}_\beta b_\alpha)_{V+A}\right] \qquad (1.15)$$

and G_f is Fermi constant and $\xi_q = V_{qd}V_{qs}^*$ with matrix V: the Cabibbo-Kobayashi-Maskawa matrix. Here μ is the renormalization point of QCD. The renormalization point dependence is separated in the operator product expansion technique. The coefficients, $A(\frac{m_W}{\mu},g)$, so called Wilson coefficients have the scale dependence. On the other hand, local operators do not have the scale dependence, but its matrix elements should have the dependence which cancel the dependence of Wilson coefficient. In this expansion, the strong interaction is split into two parts: the high momentum ($>\mu$) gluon exchange and the rest. The former is included in a Wilson coefficient in a perturbation theory. The rest part should be taken in the calculation of the matrix element of the local operators. Therefore, μ is taken as same order to energy scale of the process.

Wilson coefficients are calculated in the perturbative QCD. The perturbative calculation is improved by the renormalization group technique. For example, $A^{c(\pm)}$ obeys the renormalization group equation

$$\left(\mu\frac{\partial}{\partial\mu} + \beta(g)\frac{\partial}{\partial g} - \gamma^{(\pm)}\right) A^{c\pm}\left(\frac{m_W}{\mu},g\right) = 0 . \qquad (1.16)$$

This equation can be solved by defining the running coupling constant $\bar{g}$. The solution is written as

$$A^{c(\pm)}\left(\frac{m_W}{\mu}, g\right) = \exp\left[-\int_g^{\bar{g}(\frac{m_W}{\mu})} \frac{\gamma^{\pm}(t)}{\beta(t)} dt\right] A^{c\pm}\left(1, \bar{g}\left(\frac{m_W}{\mu}, g\right)\right) \qquad (1.17)$$

$$= \left[\frac{\alpha(m_W^2)}{\alpha'(\mu^2)}\right]^{a'(\pm)} A^{c\pm}\left(1, \bar{g}\left(\frac{m_W}{\mu}, g\right)\right) \qquad (1.18)$$

where t and $a'^{(\pm)}$ are defined

$$-\frac{\gamma^{\pm}(t)}{\beta(t)} = \frac{2a'^{(\pm)}}{t} + \text{finite term at t=0} . \qquad (1.19)$$

This equation means that we can get $A\left(\frac{m_W}{\mu}, g\right)$ by calculating the coefficient A for renormalization point $\mu = m_W$ with different coupling constant $\bar{g}$. In QCD, coupling $\bar{g}(\frac{m_W}{\mu}, g)$ is smaller than g for the μ smaller than m_W. Therefore if we calculate the $A\left(1, \bar{g}(\frac{m_W}{\mu}, g)\right)$ perturbatively instead of $A\left(\frac{m_W}{\mu}, g\right)$, the perturbative calculation is improved.

In the same way, the Wilson coefficient A_i^t is given as

$$A_i^t\left(\frac{m_W}{\mu}, g\right) = \exp\left[-\int_g^{\bar{g}(\frac{m_W}{\mu})} dt \frac{\gamma_{ij}(t)}{\beta(t)}\right] A_j^t\left(1, \bar{g}\left(\frac{m_W}{\mu}, g\right)\right) \qquad (1.20)$$

$$= V_{ik}\left[\left(\frac{\alpha(m_W^2)}{\alpha'(\mu^2)}\right)^{a'}\right]_k V_{kj}^- A_j^t\left(1, \bar{g}\left(\frac{m_W}{\mu}, g\right)\right) \qquad (1.21)$$

where V is the matrix which diagonalizes the anomalous dimension matrix of O_i and

$$\left[\left(\frac{\alpha(m_W^2)}{\alpha'(\mu^2)}\right)^{a'}\right] = \left(\left(\frac{\alpha(m_W^2)}{\alpha'(\mu^2)}\right)^{a'_1}, \left(\frac{\alpha(m_W^2)}{\alpha'(\mu^2)}\right)^{a'_2}, \cdots\right)^t . \qquad (1.22)$$

Paschos, et al. calculate the exponents a' in one loop approximation. And they determine coefficients $A\left(1, \bar{g}(\frac{m_W}{\mu}, g)\right)$ so that these coefficients correspond to the following form of the Hamiltonian

$$\frac{G_f}{\sqrt{2}}\left[\xi_u(\bar{s}_\alpha u_\alpha)_{V-A}(\bar{u}_\beta d_\beta)_{V-A} + \xi_c(\bar{s}_\alpha c_\alpha)_{V-A}(\bar{c}_\beta d_\beta)_{V-A}\right] + H_{peng}^{top} . \qquad (1.23)$$

The first term is a pure weak interaction at low-momentum transfer. This term contains $\Delta I = 3/2$ component as well as $\Delta I = 1/2$ component. The second term, H_{peng}^{top}, represents the result of one loop QCD correction that is produced by a so-called penguin diagram with the top quark in the intermediate line, which is shown in Fig 1.1, and is calculated as

$$H_{peng}^{top} = -\frac{G_f}{\sqrt{2}} \frac{\alpha_s(m_W^2)}{12\pi} F_t \xi_t \bar{d}\gamma_\mu(1 - \gamma_5)\lambda^a s \sum_f \bar{q}_f\gamma_\mu\lambda^a q_f \qquad (1.24)$$
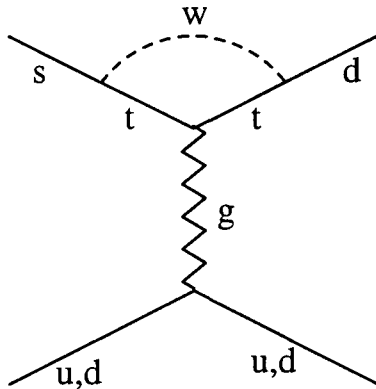
Figure 1.1: Penguin diagram with the top quark in the intermediate line.

where F_t is the structure function resulting from the loop integration. This term is needed because the top quark is heavier than the W-boson.

Using these a' and $A\left(1, \bar{g}(\frac{m_W}{\mu}, g)\right)$ the effective Hamiltonian for five quark flavors theory is obtained. The matrix elements of this effective Hamiltonian have to be evaluated in an effective theory of strong interaction with five quark flavors and coupling $g' = \bar{g}(\frac{m_W}{\mu}, g)$.

If the process has the energy scale larger than the charm quark mass but smaller than bottom quark one, the effective Hamiltonian for four-flavor theory can be obtained. It can be obtained by starting from the above Hamiltonian for five-flavor theory. The new local operators P and new Wilson coefficients B are introduced as

$$\langle | O_c^{(\pm)} | \rangle_{\text{5-flavor theory}} = B^{c(\pm)} \left(\frac{m_b}{\mu}, g'\right) \langle | O_c^{(\pm)} | \rangle_{\text{4-flavor theory}} \qquad (1.25)$$

$$\langle | O_i | \rangle_{\text{5-flavor theory}} = \sum_j B_{ij} \left(\frac{m_b}{\mu}, g'\right) \langle | P_j | \rangle_{\text{4-flavor theory}} \qquad (1.26)$$

where the local oparators are defined by

$$P_1 = (\bar{s}_\alpha d_\alpha)_{V-A}(\bar{u}_\beta u_\beta)_{V-A} \qquad (1.27)$$

$$P_2 = (\bar{s}_\alpha d_\beta)_{V-A}(\bar{u}_\beta u_\alpha)_{V-A} \qquad (1.28)$$

$$P_3 = (\bar{s}_\alpha d_\alpha)_{V-A}\left[(\bar{u}_\beta u_\beta)_{V-A} + \cdots + (\bar{c}_\beta c_\beta)_{V-A}\right] \qquad (1.29)$$

$$P_4 = (\bar{s}_\alpha d_\beta)_{V-A}\left[(\bar{u}_\beta u_\alpha)_{V-A} + \cdots + (\bar{c}_\beta c_\alpha)_{V-A}\right] \qquad (1.30)$$

$$P_5 = (\bar{s}_\alpha d_\alpha)_{V-A}\left[(\bar{u}_\beta u_\beta)_{V+A} + \cdots + (\bar{c}_\beta c_\beta)_{V+A}\right] \qquad (1.31)$$

$$P_6 = (\bar{s}_\alpha d_\beta)_{V-A}\left[(\bar{u}_\beta u_\alpha)_{V+A} + \cdots + (\bar{c}_\beta c_\alpha)_{V+A}\right] . \qquad (1.32)$$

The Wilson coefficients B are calculated in a renormalization-group improved perturbation theory. using the following boundary values

$$B^{c(\pm)}\left(1, \bar{g}'\left(m_b/\mu, g'\right)\right) = 1, \qquad B_{kl}\left(1, \bar{g}'\left(m_b/\mu, g'\right)\right) = \delta_{kl} . \tag{1.33}$$

Then the resulting effective Hamiltonian for four-flavor theory is written as

$$
\begin{aligned}
H_{eff} = &-\frac{G_f}{\sqrt{2}}\left\{\xi_c A^{c(+)}\left(\frac{m_W}{m_b}, g\right) B^{c(+)}\left(\frac{m_b}{\mu}, g'\right) O_c^+ \right.\\
&+ \xi_c A^{c(-)}\left(\frac{m_W}{m_b}, g\right) B^{c(-)}\left(\frac{m_b}{\mu}, g'\right) O_c^- \\
&\left.+ \xi_t \sum_{i=1}^{6} A_i^t\left(\frac{m_W}{m_b}, g\right) B_{ij}^t\left(\frac{m_b}{\mu}, g'\right) P_j\right\} .
\end{aligned}
\tag{1.34}
$$

The matrix elements of this effective Hamiltonian have to be evaluated in an effective theory of strong interaction with four quark flavors and coupling $g'' = \bar{g}'(\frac{m_b}{\mu}, g')$.

The energy scale for the hyperon decay is several hundred MeV, which is smaller than the charm quark mass. The effective Hamiltonian for this low energy scale is calculated by starting from the above Hamiltonian for four quark flavor theory. The resulting effective Hamiltonian for three-flavor theory is written as

$$H_{eff} = -\frac{G_f}{\sqrt{2}}\sum_{r=1r\neq4}^{6}\left(\xi_t C_r^t + \xi_c C_r^c\right) Q_r \tag{1.35}$$

where the local operators are defined by

$$Q_1 = (\bar{s}_\alpha d_\alpha)_{V-A}(\bar{u}_\beta u_\beta)_{V-A} \tag{1.36}$$

$$Q_2 = (\bar{s}_\alpha d_\beta)_{V-A}(\bar{u}_\beta u_\alpha)_{V-A} \tag{1.37}$$

$$Q_3 = (\bar{s}_\alpha d_\alpha)_{V-A}\left[(\bar{u}_\beta u_\beta)_{V-A} + \cdots + (\bar{s}_\beta s_\beta)_{V-A}\right] \tag{1.38}$$

$$Q_5 = (\bar{s}_\alpha d_\alpha)_{V-A}\left[(\bar{u}_\beta u_\beta)_{V+A} + \cdots + (\bar{s}_\beta s_\beta)_{V+A}\right] \tag{1.39}$$

$$Q_6 = (\bar{s}_\alpha d_\beta)_{V-A}\left[(\bar{u}_\beta u_\alpha)_{V+A} + \cdots + (\bar{s}_\beta s_\alpha)_{V+A}\right] \tag{1.40}$$

and Wilson coefficients are calculated as

$$
\begin{aligned}
C_r^c = \frac{1}{2}&\left\{\left[X_{rq}\left(\frac{\alpha''(m_c{}^2)}{\alpha'''(\mu^2)}\right)^{a_q'''} X_{rq}^{-1} D_p^{(+)}\right]\left(\frac{\alpha'(m_b{}^2)}{\alpha''(m_c{}^2)}\right)^{a''(+)}\left(\frac{\alpha(m_W{}^2)}{\alpha'(m_b{}^2)}\right)^{a'(+)} A^{c(+)}(1, \bar{g})\right.\\
&\left.+ \left[X_{rq}\left(\frac{\alpha''(m_c{}^2)}{\alpha'''(\mu^2)}\right)^{a_q'''} X_{rq}^- D_p^{(-)}\right]\left(\frac{\alpha'(m_b{}^2)}{\alpha''(m_c{}^2)}\right)^{a''(-)}\left(\frac{\alpha(m_W{}^2)}{\alpha'(m_b{}^2)}\right)^{a'(-)} A^{c(-)}(1, \bar{g})\right\}
\end{aligned}
$$

$$C_r^t = \frac{1}{2} \sum_{k,n} \left[\sum_{p,q} X_{rq} \left(\frac{\alpha''(m_c{}^2)}{\alpha'''(\mu^2)} \right)^{a_q'''} X_{qp}^{-1} D_n^p \right] \qquad (1.41)$$

$$\left[\sum_{l,m} W_{nm} \left(\frac{\alpha'(m_b{}^2)}{\alpha''(m_c)} \right)^{a_m''} W_{ml}^{-1} E_l^k \right] \left[\sum_{i,j} V_{kj} \left(\frac{\alpha(m_W{}^2)}{\alpha'(m_b^2)} \right)^{a_j'} V_{ji}^{-1} A_i^t(1, \bar{g}) \right] \qquad (1.42)$$

where V, W and X are the matrix which diagonalizes the anomalous dimension matrix of local operators, and the boundary values are determined as $D_p^{\pm} = (\pm 1, 1, 0, 0, 0)$, $E_i^l = \delta_{il}$ $D_n^p = \delta_{np}$ for $n \neq 4$ or $(-1, 1, 1, 0, 0)$ for n=4, $A^{c(\pm)} \left(1, \bar{g}(\frac{m_W}{\mu}, g) \right) = 1$ and $A^t \left(1, \bar{g}(\frac{m_W}{\mu}, g) \right) = \left(0, \ 2, \ -\frac{1}{3} \frac{\alpha_s(m_W^2)}{12\pi} F_t, \ \frac{\alpha_s(m_W^2)}{12\pi} F_t, \ -\frac{1}{3} \frac{\alpha_s(m_W^2)}{12\pi} F_t, \ \frac{\alpha_s(m_W^2)}{12\pi} F_t \ \right)$. The matrix elements of this effective Hamiltonian have to be evaluated in an effective theory of strong interaction with three quark flavors and coupling $\bar{g}$, which is the running coupling in low energy scale.

The numerical values of these Wilson coefficients C_r^c and C_r^t are listed in ref.[5]. The most prominent feature of this effective Hamiltonian is that the QCD correction enhances the $\Delta I = 1/2$ component and suppresses the $\Delta I = 3/2$ component. This Hamiltonian has been used for calculations of nonleptonic decay of strange mesons and baryons [2, 13, 14, 15]. It is found that although the effective Hamiltonian gives significant $\Delta I = 1/2$ enhancement, agreement to experiment is not always achieved quantitatively.

This effective Hamiltonian is being used for calculating the $\Lambda N \rightarrow NN$ transition potential induced by the direct quark mechanism.

1.3 Constituent quark picture of hadron

In this section we overview the constituent quark picture of hadron.

At the intermediate energy scale, we have a so called constituent quark picture of hadrons. In this picture, a hadron is a bound state of so called constituent quarks, which are quarks with mass about 300 MeV or 500 MeV. This simple picture can reproduce the mass spectrum and the electro-magnetic properties of hadrons. Beside this, the weak decays of hyperons or strange mesons are the processes at intermediate energy, and must be understood in a such model.

At present, the relation between the constituent quark picture and QCD is not clear. Though, several features of this picture seem to be consistent to QCD. It is pointed out that the simple vacuum of this picture may be related to the simple or trivial vacuum of the light front QCD [16]. In the light front formalism, the vacuum does not contain particle anti-particle pair and the Fock vacuum is an eigenstate of the light cone Hamiltonian. It is also pointed out that the constituent quarks are quarks in the chiral symmetry breaking phase of QCD. This situation is well demonstrated in the Nambu-Jona-Lasinio model whose Lagrangian density is, for instance [17],

$$\mathcal{L} = \bar{\psi} i \partial_\mu \gamma_\mu \psi + \frac{G_s}{2} \sum_{a=0}^{8} [(\bar{\psi}\lambda^a\psi)^2 + (\bar{\psi}\lambda^a i\gamma_5\psi)^2] \ . \tag{1.43}$$

When the contact interaction is strong enough, the chiral symmetry is spontaneously broken and quarks acquire a finite mass.

In the constituent quark picture, mesons are bound states of strongly correlated constituent quark anti-constituent-quark pair. Mesons are well studied in the NJL model. Their mass, decay constant and coupling to constituent quarks are obtained by calculating the diagram in Fig 1.2.

Baryons are bound states of three constituent quarks in the constituent quark picture. Baryons are also studied in the NJL model. However, the nonrelativistic picture is often employed [18]. For ground state baryon, the following totally antisymmetric wave function is often used.

$$\phi = \phi^{\text{color}} \phi^{\text{orbital}} \phi^{\text{flavor-spin}} \tag{1.44}$$
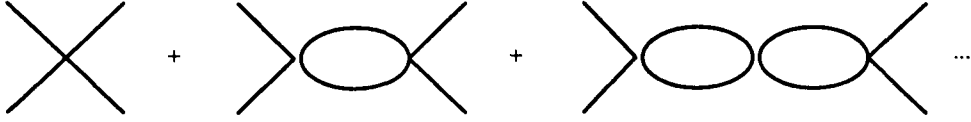
15

Figure 1.2: The RPA diagrams for the quark anti-quark scattering.

$$\phi^{\text{color}} = \frac{1}{\sqrt{6}}(RBG + BGR + GRB - RGB - BRG - GBR) \qquad (1.45)$$

$$\phi^{\text{orbital}} = Ne^{-\frac{1}{2b^2}\left(r_1 - \frac{r_1 + r_2 r_3}{3}\right)}e^{-\frac{1}{2b^2}\left(r_2 - \frac{r_1 + r_2 r_3}{3}\right)}e^{-\frac{1}{2b^2}\left(r_3 - \frac{r_1 + r_2 r_3}{3}\right)} \qquad (1.46)$$

$$\phi^{\text{flavor spin}} = SU(6)\text{wave function} \qquad (1.47)$$

This wave function ϕ is color singlet, orbital symmetric and spin-flavor symmetric. The symmetric spin flavor wave functions are known as the $SU(6)$ wave function, which are given in Table 1.1. The flavor $SU(3)$ breakings are not taken into account in these wave functions.

Multi-baryon systems can be described in a constituent quark picture by using the above single baryon wave function. It is called quark cluster model. In this model, the constituent quark component of the system is given by multiplying the single baryon wave functions and antisymmetrizing them about permutation of quarks. For example, a two baryon system which contain six constituent quarks, is described by the wave function

$$|BB'\rangle = \mathcal{A}^6|\phi_1\phi_2\chi(\vec{r}_1, \vec{r}_2)\rangle . \qquad (1.48)$$

Here, the function ϕ is the single baryon wave function and the function $\chi(\vec{r}_1, \vec{r}_2)$ is an orbital wave function of system. The Schrödinger equation for $\chi(\vec{r}_1, \vec{r}_2)$ is solved by the Resonating Group Method(RGM). It has been shown that the one gluon exchange force among constituent quarks reproduces the two nucleon short-range repulsion successfully [19, 20, 21, 22].

This quark cluster model is being used for calculating the $\Lambda N \to NN$ transition potential induced by the direct quark mechanism.

Table 1.1: SU(6) wave function

$$|p \uparrow \rangle \quad = \quad \frac{1}{3\sqrt{2}} \{ \quad (uud)(2(++-)-(+-+)-(-++))$$
$$(duu)(2(-++)-(++-)-(+-+))$$
$$(udu)(2(+-+)-(-++)-(++-)) \}$$

$$|n \uparrow \rangle \quad = \quad -\frac{1}{3\sqrt{2}} \{ \quad (ddu)(2(++-)-(+-+)-(-++))$$
$$(udd)(2(-++)-(++-)-(+-+))$$
$$(dud)(2(+-+)-(-++)-(++-)) \}$$

$$|\Lambda \uparrow \rangle \quad = \quad \frac{1}{2\sqrt{3}} \{ \quad ((uds)-(dus))((+-+)-(-++))$$
$$((sud)-(sdu))((++-)-(+-+))$$
$$((dsu)-(usd))((-++)-(++-)) \}$$

$$|\Sigma^+ \uparrow \rangle \quad = \quad \frac{1}{3\sqrt{2}} \{ \quad (uus)(2(++-)-(+-+)-(-++))$$
$$(suu)(2(-++)-(++-)-(+-+))$$
$$(usu)(2(+-+)-(-++)-(++-)) \}$$

$$|\Sigma^0 \uparrow \rangle \quad = \quad \frac{1}{6} \{ \quad ((uds)+(dus))(2(++-)-(+-+)-(-++))$$
$$((sud)+(sdu))(2(-++)-(++-)-(+-+))$$
$$((dsu)+(usd))(2(+-+)-(-++)-(++-)) \}$$

$$|\Sigma^- \uparrow \rangle \quad = \quad \frac{1}{3\sqrt{2}} \{ \quad (dds)(2(++-)-(+-+)-(-++))$$
$$(sdd)(2(-++)-(++-)-(+-+))$$
$$(dsd)(2(+-+)-(-++)-(++-)) \}$$

$$|\Xi^0 \uparrow \rangle \quad = \quad -\frac{1}{3\sqrt{2}} \{ \quad (ssu)(2(++-)-(+-+)-(-++))$$
$$(uss)(2(-++)-(++-)-(+-+))$$
$$(sus)(2(+-+)-(-++)-(++-)) \}$$

$$|\Xi^- \uparrow \rangle \quad = \quad -\frac{1}{3\sqrt{2}} \{ \quad (ssd)(2(++-)-(+-+)-(-++))$$
$$(dss)(2(-++)-(++-)-(+-+))$$
$$(sds)(2(+-+)-(-++)-(++-)) \}$$

1.4 Y-N interaction in nuclei

In this section we overview the hyperon-nucleon interaction in nuclei.

The one boson exchange (OBE) models for hyperon nucleon interaction have been proposed by the Nijmegen group [23]. There are three models: model D, model F and model soft-core. The inter-baryon interactions are assumed to be mediated by the pseudo-scalar, vector and scalar meson nonets. In these models NN and YN systems are connected by the $SU(3)$ symmetry relations. In fact, the $SU(3)$-scalar baryon-meson couplings are constructed for the baryon octet and the meson nonet. For example, pseudo scalar part is

$$
\begin{aligned}
H_{PS} = {} & g_8 \bar{N}\tau N\pi + \left\{ \frac{4\alpha-1}{\sqrt{3}} g_8 \cos\theta - g_1 \sin\theta \right\} \bar{N}N\eta \\
& -\frac{2\alpha+1}{\sqrt{3}} g_8 (\bar{N}\Lambda K + \bar{\Lambda}N\bar{K}) + (1-2\alpha)g_8 (\bar{\Sigma}\tau N\bar{K} + \bar{N}\tau\Sigma K) \\
& +2i\alpha g_8 (\bar{\Sigma}\times\Sigma)\pi + \left\{ \frac{2}{\sqrt{3}}(1-\alpha)g_8\cos\theta - g_1\sin\theta \right\} \bar{\Sigma}\Sigma\eta \\
& +\frac{2}{\sqrt{3}}(1-\alpha)g_8(\bar{\Lambda}\Sigma + \bar{\Sigma}\Lambda)\pi - \left\{ \frac{2}{\sqrt{3}}(1-\alpha)g_8\cos\theta + g_1\sin\theta \right\} \bar{\Lambda}\Lambda\eta \\
& +(2\alpha-1)g_8\bar{\Xi}\tau\Xi\pi - \left\{ \frac{2\alpha+1}{\sqrt{3}}g_8\cos\theta + g_1\sin\theta \right\} \bar{\Xi}\Xi\eta \\
& +\frac{4\alpha-1}{\sqrt{3}}g_8(\bar{\Xi}\Lambda K_c + \bar{\Lambda}\Xi\bar{K}_c) - g_8(\bar{\Sigma}\tau\Xi\bar{K}_c + \bar{\Xi}\tau\Sigma K_c) \\
& +\left\{ g_1\cos\theta + \frac{4\alpha-1}{\sqrt{3}}g_8\sin\theta \right\} \bar{N}N\eta' + \left\{ g_1\cos\theta + \frac{2}{\sqrt{3}}(1-\alpha)g_8\sin\theta \right\} \bar{\Lambda}\Lambda\eta' \\
& +\left\{ g_1\cos\theta + \frac{2}{\sqrt{3}}(1-\alpha)g_8\sin\theta \right\} \bar{\Sigma}\Sigma\eta' + \left\{ g_1\cos\theta - \frac{2\alpha+1}{\sqrt{3}}g_8\sin\theta \right\} \bar{\Xi}\Xi\eta'
\end{aligned}
\tag{1.49}
$$

here spatial coupling $\bar{B}'i\gamma_5 BM$ is assumed.

The exchange of a meson induces a transition potential. In the model D and model F, the hard cores are introduced to cut off the inner part of the potential. The coupling constants and the hard core radii in these models are determined by utilizing rich NN data as well as very limited YN data.

It is known that the baryon-baryon interaction in nuclear medium looks much weaker than that in free space. This is mainly because of the Pauli blocking. The Pauli blocking for intermediate and final states forbids many scattering channels and suppresses the effect

18

of the interaction. It is very convenient to derive an effective interaction in nuclear medium from that in free space. The G-matrix gives a good starting point for such an approach. In the Brueckner G-matrix theory, the YN G-matrix is defined by

$$G_{YN}(\omega) = V_{YN} + V_{YN}\frac{Q_N}{\omega - H_0}G_{YN}(\omega) \qquad (1.50)$$

where V_{YN} is a YN potential, H_0 denotes the free two baryon Hamiltonian, and Q_N is the Pauli operator. Because the non-locality in the r-representation of the G matrix is limited near the repulsive core region, an effective local G-matrix can be constructed. It is convenient to parameterize the resulting local G-matrix in order to use it in further application. Yamamoto *et al.* parameterizes the YN G-matrix as linear combination of Gaussian function [24]. Their strengths are expressed by quadratic functions of k_F, the Fermi momentum of nuclear matter. For example, the central part is expressed by three-range Gaussian,

$$G(r, k_f) = \sum_{i=1}^{3} w_i(k_f)e^{-(\frac{r}{\beta_i})^2} \qquad (1.51)$$

$$w_i(k_f) = a_i + b_i k_f + c k_f^2 \qquad (1.52)$$

where the parameters a_i, b_i and c_i are fixed for each channel. This effective interaction potential is called YNG potential (YN-Gaussian).

This effective G-matrix local potential is being used for calculating the wave function of light hypernuclei.

Chapter 2

$\Lambda N \to NN$ transition in a constituent quark picture

2.1 Meson exchange and direct quark mechanism

In this section, we consider the $\Lambda N \to NN$ transition.

The $\Lambda N \to NN$ transition has an intermediate energy scale. Therefore we would be able to reproduce this process in the constituent quark picture, if the picture is really reliable. Since a baryon has three constituent quarks, $\Lambda N \to NN$ process can be described by the diagram, for example, shown in Fig 2.1 and Fig 2.2. In the diagrams shown in Fig 2.1, a strangeness changing weak interaction and an emission of a constituent quark anti-quark pair take place in a Λ hyperon, and the pair is absorbed by a constituent quark in a nucleon. In the diagrams shown in Fig 2.2, a strangeness changing weak interaction among two constituent quarks in a totally anti-symmetric six constituent quark state, takes place.

The first picture might be well reproduced by the diagram in Fig 2.3, where the baryon is a Dirac particle and couples to, for example, the pion by a phenomenological Yukawa type vertex. This is the one called a meson exchange mechanism and has been studied well [25, 26, 27, 28, 29, 30]. Though this picture is very natural, one sees that this picture cannot be valid in the region where the two baryons overlap with each other. In such a region, the diagrams in Fig 2.2, namely direct quark process, might cause the $\Lambda N \to NN$ transition. The direct quark contribution has been ignored for a long time. We expect that
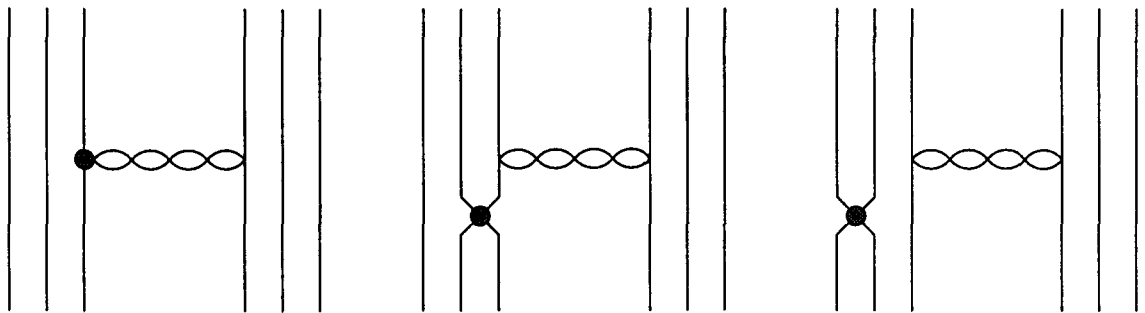
Figure 2.1: The quark diagrams for the $\Lambda N \to NN$ transition. ● denotes a weak 4-quark vertex.
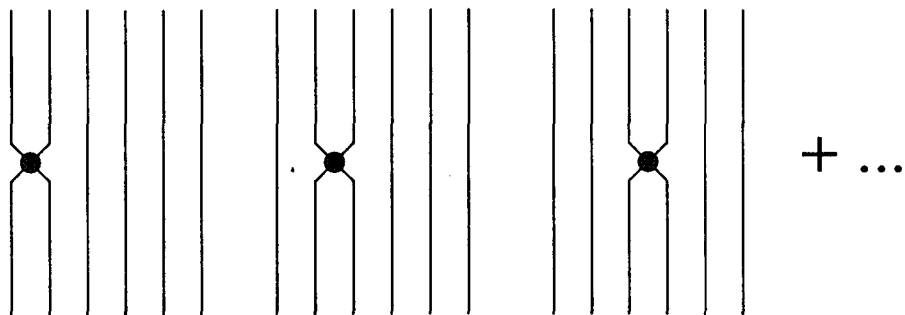
Figure 2.2: The quark diagrams for the $\Lambda N \to NN$ transition. ● denotes a weak 4-quark vertex.

the contribution of this mechanism is significant because of the large momentum transfer of $\Lambda N \to NN$ transition [31, 32, 33, 34, 35, 36].

In this thesis, we study the contribution of direct quark processes in the $\Lambda N \to NN$ transition. We construct a transition potential induced by these process. We incorporate the obtained potential in evaluating the nonmesonic decays of light hypernuclei We study and try to reproduce the nonmesonic decays of light hypernuclei.

In order to study the direct quark processes, we need the quark component of the two baryon systems and the weak interaction among the quarks. We employ the quark cluster model for the constituent quark component. And we employ the effective Hamiltonian $H_{eff}^{\Delta S=1}$ at low renormalization scale for the weak interaction Hamiltonian. We define the direct quark induced transition potential by

$$V(k,k')_{\substack{L_i,S_i,J \\ L_f,S_f,J}} = \langle NN(k', L_f, S_f, J)| H_{eff}^{\Delta S=1} |\Lambda N(k, L_i, S_i, J)\rangle . \qquad (2.1)$$

It is the first order perturbation of $H_{eff}^{\Delta S=1}$. We are to expect that a quark model contains

21
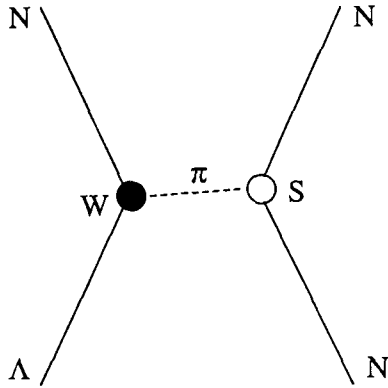
Figure 2.3: One pion exchange diagram.

the effects of the nonperturbative strong interaction which is not included in the effective Hamiltonian $H_{eff}^{\Delta S=1}$.

Note that the direct quark processes are independent from the meson exchange diagrams in our formulation because the non-relativistic formalism does not allow a pair of quark and anti-quark in the intermediate state. It should also be noticed that they have different physical meanings. The direct quark matrix elements are nonzero only at the short distance where the quark wave functions of two baryons overlap with each other, while the meson exchanges contribute at longer distances.

In the meson exchange mechanism, the one pion exchange is most important. Therefore, in this thesis, we consider the one pion exchange (OPE) and the direct quark (DQ) mechanism for the $\Lambda N \rightarrow NN$ transition. We superpose the two potentials induced by these mechanisms. A similar approach has been taken by Maltman and Shmatikov [32].

In the next section, we give the transition potential induced by the one pion exchange mechanism. In the section following the next section, we calculate the direct quark induced transition potential.

2.2 Transition potential induced by the one pion exchange mechanism

In this section the $\Lambda N \to NN$ transition potential induced by the one pion exchange mechanism is given.

The amplitude of the diagram in Fig 2.3 can be calculated in the standard Feynman rules with following vertices

$$H_{\Lambda N \pi}^w = ig_w \bar{\psi}_n (1 + \lambda \gamma_5) \pi^0 \psi_\Lambda - \sqrt{2} g_w \bar{\psi}_p (1 + \lambda \gamma_5) \pi^+ \psi_\Lambda \tag{2.2}$$

$$g_w = -2.3 \times 10^{-7}, \qquad \lambda = -6.9 \tag{2.3}$$

$$H_{NN\pi}^s = ig_s \bar{\psi}_p \gamma_5 \pi^0 \psi_p - ig_s \bar{\psi}_n \gamma_5 \pi^0 \psi_n + i\sqrt{2} g_s \bar{\psi}_p \gamma_5 \pi^+ \psi_n + i\sqrt{2} g_s \bar{\psi}_n \gamma_5 \pi^- \psi_p \tag{2.4}$$

$$g_s = 13.26 . \tag{2.5}$$

The strength g_w for the $\Lambda N \pi$ vertex is taken so as to reproduce the decay of Λ in free space. It does not contain $\Delta I = 3/2$ component. The vertex $NN\pi$ is the standard Yukawa coupling which reproduces the nuclear force. The one-pion exchange amplitude is given by

$$[\bar{u}_N g_w (1 + \lambda \gamma_5) \tau_j u_\Lambda] \frac{1}{q^2 - m_\pi^2} [\bar{u}_N g_s \gamma_5 \tau_j u_N] , \tag{2.6}$$

where u_B is the baryon spinor and q and m_π are the momentum and mass of the pion respectively. Here momentum dependence at the vertices is neglected. From this amplitude, the transition potential is obtained by performing the nonrelativistic reduction

$$V_{\mathrm{OPE}}(\vec{q}) = g_w g_s \frac{1}{2M_N} \left\{ 1 + \lambda \frac{1}{2\bar{M}} \vec{\sigma}_1 \cdot \vec{q} \right\} \frac{1}{\vec{q}^2 + \tilde{m}_\pi^2} \vec{\sigma}_2 \cdot \vec{q} \vec{\tau}_1 \cdot \vec{\tau}_2 , \tag{2.7}$$

where $\bar{M}$ is the average mass of baryons and $\tilde{m}_\pi = \sqrt{m_\pi^2 - q_0^2}$ is an effective pion mass introduced in order to take care of the finite energy transfer. Here the Breit-Fermi non-relativistic expansion up to $(m/p)^2$ is used. Therefore the change of orbital angular momentum is restricted up to 2. The coordinate-space potential is a Fourier transform of $V(\vec{q})$

$$V(\vec{r}) = \int \frac{d^3 \vec{q}}{(2\pi)^3} V(\vec{q}) e^{i\vec{q} \cdot \vec{r}} . \tag{2.8}$$

The resulting potential reads

$$V(\vec{r}) = V_c^{pc}(\vec{r}) + V_t^{pc}(\vec{r}) + V^{pv}(\vec{r}) \tag{2.9}$$

23

where

$$V_c^{pc}(\vec{r}) \;=\; -\lambda \frac{g_w g_s}{4\pi} \frac{1}{4 M_n \bar{M}} \tilde{m}_\pi^3 \frac{e^{-\tilde{m}_\pi r}}{\tilde{m}_\pi r} \frac{\vec{\sigma_1} \cdot \vec{\sigma_2}}{3} \vec{\tau_1} \cdot \vec{\tau_2} \tag{2.10}$$

$$V_t^{pc}(\vec{r}) \;=\; -\lambda \frac{g_w g_s}{4\pi} \frac{1}{4 M_n \bar{M}} \tilde{m}_\pi^3 \frac{e^{-\tilde{m}_\pi r}}{\tilde{m}_\pi r} \left(\frac{1}{3} + \frac{1}{\tilde{m}_\pi r} + \frac{1}{\tilde{m}_\pi^2 r^2} \right) S_{12}(\hat{r}) \vec{\tau_1} \cdot \vec{\tau_2} \tag{2.11}$$

$$V^{pv}(\vec{r}) \;=\; i \frac{g_w g_s}{4\pi} \frac{1}{2 M_n} \tilde{m}_\pi^2 \frac{e^{-\tilde{m}_\pi r}}{\tilde{m}_\pi r} \left(1 + \frac{1}{\tilde{m}_\pi r} \right) \vec{\sigma_2} \cdot \hat{r} \, \vec{\tau_1} \cdot \vec{\tau_2} \tag{2.12}$$

$$S_{12}(\hat{r}) \;=\; 3(\vec{\sigma}_1 \cdot \hat{r})(\vec{\sigma}_2 \cdot \hat{r}) - (\vec{\sigma}_1 \cdot \vec{\sigma}_2) \; . \tag{2.13}$$

We list the one pion exchange potential for $\Lambda N \to NN$ transition starting from the relative S-state in Table 2.1. The function which appear in the table are defined by

$$f(r) \;=\; -\frac{g_w g_s}{4\pi} \frac{\tilde{m}_\pi}{2\bar{M}} \tilde{m}_\pi \frac{e^{-\tilde{m}_\pi r}}{\tilde{m}_\pi r} \tag{2.14}$$

$$V(r) \;=\; 1 + \frac{1}{\tilde{m}_\pi r} \tag{2.15}$$

$$T(r) \;=\; \frac{1}{3} + \frac{1}{\tilde{m}_\pi r} + \frac{1}{\tilde{m}_\pi^2 r^2} \; . \tag{2.16}$$

Here the matrix elements

$$\langle nn(I=1) | \, \vec{\tau}_1 \cdot \vec{\tau}_2 \, | \Lambda n \rangle \;=\; 1 \tag{2.17}$$

$$\langle pn(I=1) | \, \vec{\tau}_1 \cdot \vec{\tau}_2 \, | \Lambda p \rangle \;=\; \frac{1}{\sqrt{2}} \tag{2.18}$$

$$\langle pn(I=0) | \, \vec{\tau}_1 \cdot \vec{\tau}_2 \, | \Lambda p \rangle \;=\; -\frac{3}{\sqrt{2}} \tag{2.19}$$

are used.

This potential being used for calculating nonmesonic decays of light hypernuclei.

24

Table 2.1: One pion exchange induced transition potential

		spin-orbital	I_{NN}	Potential
a_p	$p\Lambda \rightarrow pn$	$^1S_0 \rightarrow {}^1S_0$	1	$-\dfrac{1}{\sqrt{2}}\lambda\dfrac{\tilde{m}_\pi}{2\bar{M}}f(r)$
b_p		$\rightarrow {}^3P_0$	1	$-\dfrac{1}{\sqrt{2}}iV(r)f(r)\dfrac{1}{2}(\vec{\sigma_1}-\vec{\sigma_2})\cdot\hat{r}$
c_p		$^3S_1 \rightarrow {}^3S_1$	0	$-\dfrac{1}{\sqrt{2}}\lambda\dfrac{\tilde{m}_\pi}{2\bar{M}}f(r)$
d_p		$\rightarrow {}^3D_1$	0	$-6\lambda\dfrac{\tilde{m}_\pi}{2\bar{M}}T(r)f(r)\dfrac{\sqrt{2}}{4}S_{12}(\hat{r})$
e_p		$\rightarrow {}^1P_1$	0	$-\sqrt{\dfrac{3}{2}}iV(r)f(r)\dfrac{\sqrt{3}}{2}(\vec{\sigma_1}-\vec{\sigma_2})\cdot\hat{r}$
f_p		$\rightarrow {}^3P_1$	1	$\sqrt{\dfrac{1}{3}}iV(r)f(r)\dfrac{\sqrt{6}}{4}(\vec{\sigma_1}+\vec{\sigma_2})\cdot\hat{r}$
a_n	$n\Lambda \rightarrow nn$	$^1S_0 \rightarrow {}^1S_0$	1	$-\lambda\dfrac{\tilde{m}_\pi}{2\bar{M}}f(r)$
b_n		$\rightarrow {}^3P_0$	1	$-iV(r)f(r)\dfrac{1}{2}(\vec{\sigma_1}-\vec{\sigma_2})\cdot\hat{r}$
f_n		$^3S_1 \rightarrow {}^3P_1$	1	$\sqrt{\dfrac{2}{3}}iV(r)f(r)\dfrac{\sqrt{6}}{4}(\vec{\sigma_1}+\vec{\sigma_2})\cdot\hat{r}$

2.3 Transition potential induced by the direct quark mechanism

In this section we calculate the $\Lambda N \to NN$ transition potential induced by the direct quark mechanism.

2.3.1 Calculation

The direct quark transition potential is defined by

$$V(k, k')_{\substack{L_i, S_i, J \\ L_f, S_f, J}} = \langle NN(k', L_f, S_f, J)| H_{eff}^{\Delta S=1} |\Lambda N(k, L_i, S_i, J)\rangle . \tag{2.20}$$

First, we carry out the non-relativistic reduction of $H_{eff}^{\Delta S=1}$. We carry out the Breit-Fermi expansion to first order in p/m. We use a set of non-relativistic operators $A1 \sim C11$ listed in Table 2.2. The Hamiltonian $H_{eff}^{\Delta S=1}$ is expressed in a linear combination of $\sum_{i<j}^{6} A1_{ij} \sim \sum_{i<j}^{6} C11_{ij}$. The vectors $\vec{q}_{ij}$ and $\vec{P}_i$ are defined by

$$\vec{q}_{ij} = \vec{p_i'} - \vec{p_i} = \vec{p_j} - \vec{p_j'} \qquad \vec{P}_i = \frac{\vec{p_i} + \vec{p_i'}}{2} \tag{2.21}$$

where $\vec{p_i}$ denotes the momentum of the i-th quark. In Table 2.2, the color operator is suppressed, that is unity. Among those operators, the operators $A1, A2, B1, B2, C1$ and $C2$ are parity conserving, while the others are of first order in p/m and parity violating. These operators are symmetric in subscripts i and j. Because we truncate the expansion at p/m, the change of the relative orbital angular momentum, ΔL, is restricted to 0 or ± 1, namely no tensor transition is allowed. In the present calculation, we restrict our initial state to $L = 0$ and 1. Table 2.3 shows 24 possible combinations of L, S, J, and I for the initial and final states. Note that the transition between $^1P_1$ and $^3P_1$ vanishes because the spin change operator should change the parity as well.

Matrix elements of $\sum_{i<j}^{6} A1_{ij} \sim \sum_{i<j}^{6} C11$ are calculated for the quark cluster model wave function. Under the condition that $|\phi\phi\chi\rangle$ is totally antisymmetric for the exchange $\{1,2,3\} \leftrightarrow \{4,5,6\}$, the matrix element, for instance

$$\langle B_3 B_4| \sum_{i<j}^{6} A1_{ij} |B_1 B_2\rangle, \tag{2.22}$$

Table 2.2: The set of nonrelativistic operators to expand the Hamiltonian $H_{eff}^{\Delta S=1}$

$$A1_{ij} \;=\; [(d^\dagger s)_i(u^\dagger u)_j + (u^\dagger u)_i(d^\dagger s)_j] \;\otimes\; 1 \;\otimes\; 1$$

$$A2_{ij} \;=\; + \;\otimes\; (\vec{\sigma}_i \cdot \vec{\sigma}_j) \;\otimes\; 1$$

$$A3_{ij} \;=\; + \;\otimes\; (\vec{\sigma}_i - \vec{\sigma}_j) \;\otimes\; (\vec{q}_{ij})$$

$$A4_{ij} \;=\; + \;\otimes\; \;\otimes\; \left(\vec{P}_i - \vec{P}_j\right)$$

$$A5_{ij} \;=\; - \;\otimes\; \;\otimes\; \left(\vec{P}_i + \vec{P}_j\right)$$

$$A6_{ij} \;=\; + \;\otimes\; i\left(\vec{\sigma}_i \times \vec{\sigma}_j\right) \;\otimes\; (\vec{q}_{ij})$$

$$A7_{ij} \;=\; + \;\otimes\; \;\otimes\; \left(\vec{P}_i - \vec{P}_j\right)$$

$$A8_{ij} \;=\; - \;\otimes\; \;\otimes\; \left(\vec{P}_i + \vec{P}_j\right)$$

$$A9_{ij} \;=\; - \;\otimes\; (\vec{\sigma}_i + \vec{\sigma}_j) \;\otimes\; (\vec{q}_{ij})$$

$$A10_{ij} \;=\; - \;\otimes\; \;\otimes\; \left(\vec{P}_i - \vec{P}_j\right)$$

$$A11_{ij} \;=\; + \;\otimes\; \;\otimes\; \left(\vec{P}_i + \vec{P}_j\right)$$

$$B1_{ij} \;=\; [(d^\dagger s)_i(d^\dagger d)_j + (d^\dagger d)_i(d^\dagger s)_j] \;\otimes\; 1 \;\otimes\; 1$$

$$\vdots$$

$$B11_{ij} \;=\; + \;\otimes\; (\vec{\sigma}_i + \vec{\sigma}_j) \;\otimes\; \left(\vec{P}_i + \vec{P}_j\right)$$

$$C1_{ij} \;=\; [(u^\dagger s)_i(d^\dagger u)_j + (d^\dagger u)_i(u^\dagger s)_j] \;\otimes\; 1 \;\otimes\; 1$$

$$\vdots$$

$$C11_{ij} \;=\; + \;\otimes\; (\vec{\sigma}_i + \vec{\sigma}_j) \;\otimes\; \left(\vec{P}_i + \vec{P}_j\right) \;.$$

Table 2.3: Possible $\Lambda N \to NN$ transitions when one assume that the initial $L = 0$ or 1 and $\Delta L = 0$ or ± 1.

	spin-orbital	Type	W
$p\Lambda \to pn$	$^1S_0 \to {}^1S_0$	1	1
	$\to {}^3P_0$	2	$-\sqrt{3}$
	$^3S_1 \to {}^3S_1$	3	1
	$\to {}^1P_1$	4	1
	$\to {}^3P_1$	5	$-\sqrt{2}$
	$^1P_1 \to {}^3S_1$	F	1
	$\to {}^1P_1$	G	1
	$\to {}^3D_1$	F	$-\sqrt{\frac{5}{2}}$
	$^3P_0 \to {}^1S_0$	B	$-\sqrt{3}$
	$\to {}^3P_0$	A	1
	$^3P_1 \to {}^3S_1$	C	$-\sqrt{2}$
	$\to {}^3P_1$	A	1
	$\to {}^3D_1$	C	$-\frac{\sqrt{5}}{2}$
	$^3P_2 \to {}^3P_2$	A	1
	$\to {}^1D_2$	B	$\sqrt{\frac{3}{2}}$
	$\to {}^3D_2$	C	$-\frac{3}{2}$
$n\Lambda \to nn$	$^1S_0 \to {}^1S_0$	6	1
	$\to {}^3P_0$	7	$-\sqrt{3}$
	$^3S_1 \to {}^3P_1$	8	$-\sqrt{2}$
	$^3P_0 \to {}^1S_0$	I	$-\sqrt{3}$
	$\to {}^3P_0$	H	1
	$^3P_1 \to {}^3P_1$	H	1
	$^3P_2 \to {}^3P_2$	H	1
	$\to {}^1D_2$	I	$-\sqrt{\frac{3}{2}}$

is equal to

$$\frac{6}{N}\langle\phi\phi\chi|\,A1_{12}\,|\phi\phi\chi\rangle + \frac{9}{N}\langle\phi\phi\chi|\,A1_{36}\,|\phi\phi\chi\rangle$$

$$-\frac{18}{N}\langle\phi\phi\chi|\,A1_{12}P_{36}\,|\phi\phi\chi\rangle - \frac{36}{N}\langle\phi\phi\chi|\,A1_{13}P_{36}\,|\phi\phi\chi\rangle$$

$$-\frac{36}{N}\langle\phi\phi\chi|\,A1_{25}P_{36}\,|\phi\phi\chi\rangle - \frac{36}{N}\langle\phi\phi\chi|\,A1_{35}P_{36}\,|\phi\phi\chi\rangle$$

$$-\frac{9}{N}\langle\phi\phi\chi|\,A1_{36}P_{36}\,|\phi\phi\chi\rangle \tag{2.23}$$

where P_{36} represents the permutation operator, $3 \leftrightarrow 6$. Fig. 2.2 shows the diagrams corresponding to each term of eq.(2.23). Because the Hamiltonian is totally symmetric, the antisymmetrization operators $\mathcal{A}^6$ in the initial and final state can be replaced by a single P_{36} operated to the initial state. N is the normalization factor, which depends on the channel but is nearly equal to 1 in general. We factorize each matrix element in eq.(2.23) into the flavor-spin, orbital and color parts as

$$\langle\phi\phi\chi(k',L_f,S_f,J)|\,A1_{ij}(P_{36})\,|\phi\phi\chi(k,L_i,S_i,J)\rangle$$

$$= \langle\phi\phi\chi^{\text{flavor-spin}}|\,A1_{ij\ z}^{\text{flavor-spin}}(P_{36}^{\text{flavor-spin}})\,|\phi\phi\chi^{\text{flavor-spin}}\rangle$$

$$\times\langle\phi\phi\chi^{\text{orbital}}|\,A1_{ij\ z}^{\text{orbital}}(P_{36}^{\text{orbital}})\,|\phi\phi\chi^{\text{orbital}}\rangle$$

$$\times\langle\phi\phi\chi^{\text{color}}|\,1(P_{36}^{\text{color}})\,|\phi\phi\chi^{\text{color}}\rangle \times W\ . \tag{2.24}$$

The factor W is an algebraic factor required when we factorize the spin and orbital matrix elements. It is defined by

$$W = (-)^\lambda\sqrt{2\lambda+1}\sqrt{2J+1}\begin{Bmatrix} L_i & S_i & J \\ \lambda & \lambda & 0 \\ L_f & S_f & J \end{Bmatrix}\frac{\sqrt{2L_f+1}}{(L_i,\lambda,L_z,0|L_f,L_z)}\frac{\sqrt{2S_f+1}}{(S_i,\lambda,S_z,0|S_f,S_z)} \tag{2.25}$$

where λ is the ranks of the orbital or spin operator.

In Table 2.3, we label the combinations of the initial and the final spin-flavor part of $|\phi\phi\chi\rangle$ by "Type". Table 2.4 gives the spin-flavor part of $|\phi\phi\chi\rangle$ for each Type. One sees that $|\phi\phi\chi\rangle$ is totally antisymmetric under the exchange $\{1,2,3\}\leftrightarrow\{4,5,6\}$. We choose either $s_z = 0$ or 1 so that $(s_i,\lambda^s,s_z,0|s_f,s_z)$ does not vanish. Using the $SU(6)$ flavor-spin wave function for the nucleon and Λ, we can get the flavor-spin matrix element in eq (2.24).

Table 2.4: Flavor-Spin part of $|\phi\phi\chi\rangle$.

Ty.	Initial Orb.	Initial Flavor	Initial Spin	Final Orb.	Final Flavor	Final Spin
		Initial			Final	
1	S	$\frac{1}{\sqrt{2}}(p\Lambda + \Lambda p)$	$\frac{1}{\sqrt{2}}(\uparrow\downarrow - \downarrow\uparrow)$	S	$\frac{1}{\sqrt{2}}(pn + np)$	$\frac{1}{\sqrt{2}}(\uparrow\downarrow - \downarrow\uparrow)$
2		+	−	P	+	+
3		−	+	S	−	+
4		−	+	P	−	−
5		−	$\uparrow\uparrow$	P	+	$\uparrow\uparrow$
A	P	+	$\uparrow\uparrow$	P	+	$\uparrow\uparrow$
B		+	$\frac{1}{\sqrt{2}}(\uparrow\downarrow + \downarrow\uparrow)$	S	+	$\frac{1}{\sqrt{2}}(\uparrow\downarrow - \downarrow\uparrow)$
C		+	$\uparrow\uparrow$	S	−	$\uparrow\uparrow$
F		−	$\frac{1}{\sqrt{2}}(\uparrow\downarrow - \downarrow\uparrow)$	S	−	$\frac{1}{\sqrt{2}}(\uparrow\downarrow + \downarrow\uparrow)$
G		−	−	P	−	−
6	S	$\frac{1}{\sqrt{2}}(n\Lambda + \Lambda n)$	$\frac{1}{\sqrt{2}}(\uparrow\downarrow - \downarrow\uparrow)$	S	nn	$\frac{1}{\sqrt{2}}(\uparrow\downarrow - \downarrow\uparrow)$
7		+	−	P	nn	+
8		−	$\uparrow\uparrow$	P	nn	$\uparrow\uparrow$
H	P	+	$\uparrow\uparrow$	P	nn	$\uparrow\uparrow$
I		+	$\frac{1}{\sqrt{2}}(\uparrow\downarrow + \downarrow\uparrow)$	S	nn	$\frac{1}{\sqrt{2}}(\uparrow\downarrow - \downarrow\uparrow)$

In the quark model, the orbital wave function of baryon is given analytically. Therefore we can calculate the orbital matrix elements in eq (2.24). Explicit forms of these matrix elements are listed in Table 2.5 ~ Table 2.8.

The color matrix elements are given by

$$\langle \text{color-singlet} | 1 | \text{color-singlet} \rangle \quad = \quad 1, \tag{2.26}$$

$$\langle \text{color-singlet} | 1 P_{36}^{\text{color}} | \text{color-singlet} \rangle \quad = \quad 1/3. \tag{2.27}$$

Finally, by collecting above matrix elements, we obtain the direct quark transition potential.

Table 2.5: Orbital matrix elements in a quark model.

$\mathcal{O}_{ij}(P_{36})$	$\langle\ \phi\phi(2\pi)^3\delta^3(\vec{P}'-\vec{k}')|\ \mathcal{O}_{ij}(P_{36})\ |\phi\phi(2\pi)^3\delta^3(\vec{P}-\vec{k})\ \rangle$
1_{12}	$\sqrt{2\pi}^3\dfrac{1}{b^3}\dfrac{1}{k^2}\delta(k'-k)$
$1_{12}\,P_{36}$	$\dfrac{3\sqrt{6}}{4}\exp\left[-b^2(\dfrac{5}{12}k^2+\dfrac{1}{2}\vec{k}\cdot\vec{k}'+\dfrac{5}{12}k'^2)\right]$
$1_{13}\,P_{36}$	$\dfrac{24\sqrt{33}}{121}\exp\left[-b^2\dfrac{1}{33}(7k^2+12\vec{k}\cdot\vec{k}'+13k'^2)\right]$
$1_{25}\,P_{36}$	$\dfrac{3\sqrt{3}}{8}\exp\left[-b^2\dfrac{1}{6}(k^2+k'^2)\right]$
$1_{35}\,P_{36}$	$\dfrac{24\sqrt{33}}{121}\exp\left[-b^2\dfrac{1}{33}(13k^2+12\vec{k}\cdot\vec{k}'+7k'^2)\right]$
1_{36}	$\exp\left[-b^2\dfrac{1}{3}(k^2+2\vec{k}\cdot\vec{k}'+k'^2)\right]$
$1_{36}\,P_{36}$	$\exp\left[-b^2\dfrac{1}{3}(k^2+2\vec{k}\cdot\vec{k}'+k'^2)\right]$

Table 2.6: Orbital matrix elements in a quark model.

$\mathcal{O}_{ij}(P_{36})$	$\langle\ \phi\phi(2\pi)^3\delta^3(\vec{P}'-\vec{k}')|\ \mathcal{O}_{ij}(P_{36})\ |\phi\phi(2\pi)^3\delta^3(\vec{P}-\vec{k})\ \rangle$
$\vec{q}_{12}$	0
$\vec{q}_{12}\,P_{36}$	0
$\vec{q}_{13}\,P_{36}$	$\dfrac{1}{66}\left\{-36\vec{k}+12\vec{k}'\right\}\langle|\,1_{13}P_{36}\,|\rangle$
$\vec{q}_{25}\,P_{36}$	$\dfrac{1}{66}\left\{-33\vec{k}+33\vec{k}'\right\}\langle|\,1_{25}P_{36}\,|\rangle$
$\vec{q}_{35}\,P_{36}$	$\dfrac{1}{66}\left\{-12\vec{k}+36\vec{k}'\right\}\langle|\,1_{35}P_{36}\,|\rangle$
$\vec{q}_{36}$	$\dfrac{1}{66}\left\{-66\vec{k}+66\vec{k}'\right\}\langle|\,1_{36}\,|\rangle$
$\vec{q}_{36}\,P_{36}$	$\dfrac{1}{66}\left\{+22\vec{k}+22\vec{k}'\right\}\langle|\,1_{36}P_{36}\,|\rangle$

Table 2.7: Orbital matrix elements in a quark model.

$\mathcal{O}_{ij}(P_{36})$	$\langle\ \phi\phi(2\pi)^3\delta^3(\vec{P}' - \vec{k}')\vert\ \mathcal{O}_{ij}(P_{36})\ \vert\phi\phi(2\pi)^3\delta^3(\vec{P} - \vec{k})\ \rangle$
$(\vec{P}_1 - \vec{P}_2)$	0
$(\vec{P}_1 - \vec{P}_2)\ P_{36}$	0
$(\vec{P}_1 - \vec{P}_3)\ P_{36}$	$\dfrac{1}{66}\left\{+36\vec{k} - 12\vec{k}'\right\}\langle\vert\ 1_{13}P_{36}\ \vert\rangle$
$(\vec{P}_2 - \vec{P}_5)\ P_{36}$	$\dfrac{1}{66}\left\{+33\vec{k} + 33\vec{k}'\right\}\langle\vert\ 1_{25}P_{36}\ \vert\rangle$
$(\vec{P}_3 - \vec{P}_5)\ P_{36}$	$\dfrac{1}{66}\left\{-12\vec{k} + 36\vec{k}'\right\}\langle\vert\ 1_{35}P_{36}\ \vert\rangle$
$(\vec{P}_3 - \vec{P}_6)$	$\dfrac{1}{66}\left\{+22\vec{k} + 22\vec{k}'\right\}\langle\vert\ 1_{36}\ \vert\rangle$
$(\vec{P}_3 - \vec{P}_6)\ P_{36}$	$\dfrac{1}{66}\left\{-66\vec{k} + 66\vec{k}'\right\}\langle\vert\ 1_{36}P_{36}\ \vert\rangle$

Table 2.8: Orbital matrix elements in a quark model.

$\mathcal{O}_{ij}(P_{36})$	$\langle\ \phi\phi(2\pi)^3\delta^3(\vec{P}' - \vec{k}')\vert\ \mathcal{O}_{ij}(P_{36})\ \vert\phi\phi(2\pi)^3\delta^3(\vec{P} - \vec{k})\ \rangle$
$(\vec{P}_1 + \vec{P}_2)$	$\dfrac{1}{66}\left\{+22\vec{k} + 22\vec{k}'\right\}\langle\vert\ 1_{12}\ \vert\rangle$
$(\vec{P}_1 + \vec{P}_2)\ P_{36}$	$\dfrac{1}{66}\left\{+33\vec{k} - 33\vec{k}'\right\}\langle\vert\ 1_{12}P_{36}\ \vert\rangle$
$(\vec{P}_1 + \vec{P}_3)\ P_{36}$	$\dfrac{1}{66}\left\{+12\vec{k} - 48\vec{k}'\right\}\langle\vert\ 1_{13}P_{36}\ \vert\rangle$
$(\vec{P}_2 + \vec{P}_5)\ P_{36}$	0
$(\vec{P}_3 + \vec{P}_5)\ P_{36}$	$\dfrac{1}{66}\left\{-48\vec{k} + 12\vec{k}'\right\}\langle\vert\ 1_{35}P_{36}\ \vert\rangle$
$(\vec{P}_3 + \vec{P}_6)$	0
$(\vec{P}_3 + \vec{P}_6)\ P_{36}$	0

2.3.2 Result

The obtained direct quark transition potential is written in the following form [36].

$$V(k, k')_{\substack{L_i, S_i, J \\ L_f, S_f, J}} = -\frac{G_F}{\sqrt{2}} \sum_{i=1}^{7} \{V_i^f \ f(k, k')_i + V_i^g \ g(k, k')_i + V_i^h \ h(k, k')_i\} \times W \quad (2.28)$$

The $f(k, k')$, $g(k, k')$ and $h(k, k')$ are analytic functions which are given in Tables 2.9 $\sim$ 2.11. In these tables, $\delta(L_i, L_f)$, $I(L_i, L_f)$, $\exp[ij]$ and $F(L, X)$ are defined by

$$\delta(L_i, L_f) = \delta_{L_i L_f} \quad (2.29)$$

$$I(L_i, L_f) = \int Y_{L_f}^{0*}(\Omega) \cos\theta Y_{L_i}^{0}(\Omega) d\Omega \quad (2.30)$$

$$\exp[12] = \frac{3\sqrt{6}}{4} \exp\left[-b^2 \frac{5}{12}(k^2 + k'^2)\right] \quad (2.31)$$

$$\exp[13] = \frac{24\sqrt{33}}{121} \exp\left[-b^2 \frac{1}{33}(7k^2 + 13k'^2)\right] \quad (2.32)$$

$$\exp[25] = \frac{3\sqrt{3}}{8} \exp\left[-b^2 \frac{1}{6}(k^2 + k'^2)\right] \quad (2.33)$$

$$\exp[35] = \frac{24\sqrt{33}}{121} \exp\left[-b^2 \frac{1}{33}(13k^2 + 7k'^2)\right] \quad (2.34)$$

$$\exp[36] = \exp\left[-b^2 \frac{1}{3}(k^2 + k'^2)\right] \quad (2.35)$$

$$F(0, X) = 4\pi \frac{\sinh(Xb^2kk')}{Xb^2kk'} \quad (2.36)$$

$$F(1, X) = -4\pi \left(\frac{\sinh(Xb^2kk')}{X^2b^4k^2k'^2} - \frac{\cosh(Xb^2kk')}{Xb^2kk'}\right) . \quad (2.37)$$

The coefficients, V^f, V^g and V^h are numerical constant. In order to get these coefficients, we have to fix the Wilson coefficients in $H_{eff}^{\Delta S=1}$ (see eq.(1.35)) and the ratio m_s/m, where m and m_s are the constituent quark mass of the u or d quark and s quark respectively. In the present study we use one set of the Wilson coefficients given in ref. [5]. It is calculated with the renormalization point $\mu = 0.24$ GeV and top quark mass $m_t = 200$ GeV. And we employ 5/3 for m_s/m. We preset the obtained coefficients in Tables 2.12 $\sim$ 2.14.

The weak Hamiltonian which we use contains $\Delta I = 3/2$ components. In order to study the contribution of this $\Delta I = 3/2$ part, we also calculate the potential when we omit it. The transition potential in this case can be obtained by substituting the coefficients given in Table 2.15 $\sim$ Table 2.17.

Table 2.9: The functions in potential.

$$f(k, k')_1 = \frac{6}{N} \ 1 \ \delta(L_i, L_f)\sqrt{2\pi}^{-3}\frac{1}{b^3}\frac{1}{k^2}\delta(k' - k)$$

$$f(k, k')_2 = -\frac{18}{N} \ \frac{1}{3} \ \delta(L_i, L_f) \ \exp[12] \ F\left(L_i, \frac{1}{2}\right)$$

$$f(k, k')_3 = -\frac{36}{N} \ \frac{1}{3} \ \delta(L_i, L_f) \ \exp[13] \ F\left(L_i, \frac{12}{33}\right)$$

$$f(k, k')_4 = -\frac{36}{N} \ \frac{1}{3} \ \delta(L_i, L_f) \ \exp[25] \ F\left(L_i, 0\right)$$

$$f(k, k')_5 = -\frac{36}{N} \ \frac{1}{3} \ \delta(L_i, L_f) \ \exp[35] \ F\left(L_i, \frac{12}{33}\right)$$

$$f(k, k')_6 = \frac{9}{N} \ 1 \ \delta(L_i, L_f) \ \exp[36] \ F\left(L_i, \frac{2}{3}\right)$$

$$f(k, k')_7 = -\frac{9}{N} \ \frac{1}{3} \ \delta(L_i, L_f) \ \exp[36] \ F\left(L_i, \frac{2}{3}\right)$$

Table 2.10: The functions in potential.

$$g(k, k')_1 = \frac{6}{N} \ 1 \ I(L_i, L_f) \ \frac{k}{m}\sqrt{2\pi}^{-3}\frac{1}{b^3}\frac{1}{k^2}\delta(k' - k)$$

$$g(k, k')_2 = -\frac{18}{N} \ \frac{1}{3} \ I(L_i, L_f) \ \frac{k}{m} \ \exp[12] \ F\left(L_f, \frac{1}{2}\right)$$

$$g(k, k')_3 = -\frac{36}{N} \ \frac{1}{3} \ I(L_i, L_f) \ \frac{k}{m} \ \exp[13] \ F\left(L_f, \frac{12}{33}\right)$$

$$g(k, k')_4 = -\frac{36}{N} \ \frac{1}{3} \ I(L_i, L_f) \ \frac{k}{m} \ \exp[25] \ F\left(L_f, 0\right)$$

$$g(k, k')_5 = -\frac{36}{N} \ \frac{1}{3} \ I(L_i, L_f) \ \frac{k}{m} \ \exp[35] \ F\left(L_f, \frac{12}{33}\right)$$

$$g(k, k')_6 = \frac{9}{N} \ 1 \ I(L_i, L_f) \ \frac{k}{m} \ \exp[36] \ F\left(L_f, \frac{2}{3}\right)$$

$$g(k, k')_7 = -\frac{9}{N} \ \frac{1}{3} \ I(L_i, L_f) \ \frac{k}{m} \ \exp[36] \ F\left(L_f, \frac{2}{3}\right)$$

Table 2.11: The functions in potential.

$$h(k, k')_1 = \frac{6}{N} \ 1 \ I(L_i, L_f) \ \frac{k'}{m}\sqrt{2\pi}^{-3}\frac{1}{b^3}\frac{1}{k^2}\delta(k' - k)$$

$$h(k, k')_2 = -\frac{18}{N} \ \frac{1}{3} \ I(L_i, L_f) \ \frac{k'}{m} \ \exp[12] \ F\left(L_i, \frac{1}{2}\right)$$

$$h(k, k')_3 = -\frac{36}{N} \ \frac{1}{3} \ I(L_i, L_f) \ \frac{k'}{m} \ \exp[13] \ F\left(L_i, \frac{12}{33}\right)$$

$$h(k, k')_4 = -\frac{36}{N} \ \frac{1}{3} \ I(L_i, L_f) \ \frac{k'}{m} \ \exp[25] \ F\left(L_i, 0\right)$$

$$h(k, k')_5 = -\frac{36}{N} \ \frac{1}{3} \ I(L_i, L_f) \ \frac{k'}{m} \ \exp[35] \ F\left(L_i, \frac{12}{33}\right)$$

$$h(k, k')_6 = \frac{9}{N} \ 1 \ I(L_i, L_f) \ \frac{k'}{m} \ \exp[36] \ F\left(L_i, \frac{2}{3}\right)$$

$$h(k, k')_7 = -\frac{9}{N} \ \frac{1}{3} \ I(L_i, L_f) \ \frac{k'}{m} \ \exp[36] \ F\left(L_i, \frac{2}{3}\right)$$

Table 2.12: The coefficients V^f. The numbers are normalized in the unit of $\sqrt{6}$ / 660 /1296 for Type 1, 2, 3, 4, 5, A, B, C and F and in the unit of $\sqrt{3}$ / 660 /648 for Type 6, 7, 8, H and I.

Ty.	V_1^f	V_2^f	V_3^f	V_4^f	V_5^f	V_6^f	V_7^f
1	-77588.4	29011.5	-787.2	6117.8	-10195.3	39068.5	-34345.4
3	-77588.4	29011.5	-787.2	303.9	-10195.3	4185.1	538.0
G	-77588.4	-79950.0	-163442.3	-79950.0	-50544.8	-162261.5	-162261.5
A	-77588.4	-44941.4	-34614.9	-13581.0	-22070.8	-13756.8	-12855.1
6	-77588.4	29011.5	-787.2	-67.5	-10195.3	1956.7	2766.4
H	-77588.4	-44941.4	-34614.9	-13581.0	-22070.8	-9633.2	-16978.7

Table 2.13: The coefficients V^g. The numbers are normalized in the unit of $\sqrt{6}$ / 660 /1296 for Type 1, 2, 3, 4, 5, A, B, C and F and in the unit of $\sqrt{3}$ / 660 /648 for Type 6, 7, 8, H and I.

Ty.	V_1^g	V_2^g	V_3^g	V_4^g	V_5^g	V_6^g	V_7^g
2	-54.3	-297.1	15321.8	5760.4	-43.6	21392.9	-2476.8
4	-54.3	-84.6	69818.0	31586.4	1490.8	85572.9	84357.2
5	54.3	-122.8	-14966.7	-5465.2	-1767.2	-758.7	-2202.1
F	-54.3	184.6	314.9	-256.9	-6683.7	-57943.0	-52750.3
B	-54.3	214.6	166.3	-2266.7	-2239.4	-25126.8	12162.8
C	54.3	45.2	-142.0	53.9	-182.6	-1155.6	-261.3
7	-54.3	115.3	15321.8	5760.4	656.1	6823.1	12093.1
8	54.3	152.1	-14941.7	-5465.2	-1467.3	66.0	-3026.8
I	-54.3	-60.3	216.3	207.4	-2039.5	-3959.3	-9004.7

Table 2.14: The coefficients V^h. The numbers are normalized in the unit of $\sqrt{6}\ /\ 660\ /1296$ for Type 1, 2, 3, 4, 5, A, B, C and F and in the unit of $\sqrt{3}\ /\ 660\ /648$ for Type 6, 7, 8, H and I.

Ty	V_1^h	V_2^h	V_3^h	V_4^h	V_5^h	V_6^h	V_7^h
2	-54.3	-297.1	-5116.0	-4602.0	-1294.7	-28090.4	17845.1
4	-54.3	-84.6	-23274.8	-759.8	-4683.2	-43698.3	-41266.8
5	54.3	-122.8	5007.7	-586.3	4817.9	-10152.2	-6002.8
F	-54.3	184.6	0.0	13521.8	19700.0	110914.1	106694.0
B	-54.3	214.6	69.6	1436.8	6307.2	21951.0	1772.9
C	54.3	45.2	95.6	295.2	439.2	3666.7	584.1
7	-54.3	115.3	-5116.0	552.4	-1469.7	-2249.6	-7995.7
8	54.3	152.1	4907.7	444.6	4742.9	-8502.8	-7652.2
I	-54.3	-60.3	-130.4	1436.8	6257.2	9305.5	14418.4

Table 2.15: The coefficients V^f without $\Delta I = 3/2$ part. The numbers are normalized in the unit of $\sqrt{6}\ /\ 660\ /1296$ for Type 1, 2, 3, 4, 5, A, B, C and F and in the unit of $\sqrt{3}\ /\ 660\ /648$ for Type 6, 7, 8, H and I.

Ty.	V_1^f	V_2^f	V_3^f	V_4^f	V_5^f	V_6^f	V_7^f
1	-77588.4	29011.5	-787.2	1994.3	-10195.3	14327.3	-9604.2
3	-77588.4	29011.5	-787.2	303.9	-10195.3	4185.1	538.0
G	-77588.4	-79950.0	-163442.3	-79950.0	-50544.8	-162261.5	-162261.5
A	-77588.4	-44941.4	-34614.9	-13581.0	-22070.8	-11007.7	-15604.2
6	-77588.4	29011.5	-787.2	1994.3	-10195.3	14327.3	-9604.2
H	-77588.4	-44941.4	-34614.9	-13581.0	-22070.8	-11007.7	-15604.2

Table 2.16: The coefficients V^g without $\Delta I = 3/2$ part. The numbers are normalized in the unit of $\sqrt{6}$ / 660 /1296 for Type 1, 2, 3, 4, 5, A, B, C and F and in the unit of $\sqrt{3}$ / 660 /648 for Type 6, 7, 8, H and I.

Ty.	V_1^g	V_2^g	V_3^g	V_4^g	V_5^g	V_6^g	V_7^g
2	-54.3	-22.2	15321.8	5760.4	422.9	11679.7	7236.5
4	-54.3	-84.6	69818.0	31586.4	1490.8	85572.9	84357.2
5	54.3	60.5	-14950.0	-5465.2	-1567.3	-208.9	-2751.9
F	-54.3	184.6	314.9	-256.9	-6683.7	-57943.0	-52750.3
B	-54.3	31.4	199.6	-617.3	-2106.2	-11015.1	-1948.9
C	54.3	45.2	-142.0	53.9	-182.6	-1155.6	-261.3
7	-54.3	-22.2	15321.8	5760.4	422.9	11679.7	7236.5
8	54.3	60.5	-14950.0	-5465.2	-1567.3	-208.9	-2751.9
I	-54.3	31.4	199.6	-617.3	-2106.2	-11015.1	-1948.9

Table 2.17: The coefficients V^h without $\Delta I = 3/2$ part. The numbers are normalized in the unit of $\sqrt{6}$ / 660 /1296 for Type 1, 2, 3, 4, 5, A, B, C and F and in the unit of $\sqrt{3}$ / 660 /648 for Type 6, 7, 8, H and I.

Ty.	V_1^h	V_2^h	V_3^h	V_4^h	V_5^h	V_6^h	V_7^h
2	-54.3	-22.2	-5116.0	-1165.8	-1411.3	-10863.2	617.9
4	-54.3	-84.6	-23274.8	-759.8	-4683.2	-43698.3	-41266.8
5	54.3	60.5	4941.0	101.0	4767.9	-9052.6	-7102.4
F	-54.3	184.6	0.0	13521.8	19700.0	110914.1	106694.0
B	-54.3	31.4	-63.7	1436.8	6273.8	13520.7	10203.2
C	54.3	45.2	95.6	295.2	439.2	3666.7	584.1
7	-54.3	-22.2	-5116.0	-1165.8	-1411.3	-10863.2	617.9
8	54.3	60.5	4941.0	101.0	4767.9	-9052.6	-7102.4
I	-54.3	31.4	-63.7	1436.8	6273.8	13520.7	10203.2

Chapter 3

Nonmesonic decays of light hypernuclei

3.1 Nonmesonic decay rate

The total nonmesonic decay rate can be expressed in a sum of the partial decay rates.

$$\Gamma_{nm} = \sum_{ch} \Gamma_{ch} \ . \tag{3.1}$$

There are nine $\Lambda N \to NN$ channels for the light s-shell hypernuclei, which are labeled a through f in Table 3.1 according to the widely used notation [6]. Each partial decay rate can be obtained by integration

$$\Gamma_{ch} = [\# \text{ of Pair}] \times [\text{Spin Average Factor}] \times$$

$$\int \frac{d^3 k}{(2\pi)^3} \int \frac{d^3 K}{(2\pi)^3} (2\pi) \delta(E.C.) \, |\langle \Psi_{N^n} \Psi_{NN}(r_f, R; k, K) | V_{ch}(r_i, r_f) | \Psi_{N^n} \Psi_{\Lambda N}(r_i, R) \rangle|^2 \tag{3.2}$$

Here V_{ch} denote the $\Lambda N \to NN$ transition potential which corresponds to the channel ch. The state $|\Psi_{N^n} \Psi_{\Lambda N}(r_i, R)\rangle$ denotes the wave function of initial hypernuclei, where $\Psi_{\Lambda N}$ is the wave function of Λ-N system and Ψ_{N^n} is the wave function of nucleons. The state $|\Psi_{N^n} \Psi_{NN}(r_f, R; k, K)\rangle$ denotes the wave function of the final system, where Ψ_{NN} is the wave function of outgoing NN system. The function $\delta(E.C.)$ correspond to the energy conservation

$$M_{core} + M_\Lambda - B_\Lambda + M_n - B_N = M_{core} + 2M_N + \frac{K^2}{4M_N} + \frac{k^2}{2M_N} \tag{3.3}$$

Table 3.1: Nine $\Lambda N \rightarrow NN$ channels with initial $L = 0$.

label	channel		
a_p	$p\Lambda \rightarrow pn$	$^1S_0$	$\rightarrow {}^1S_0$
b_p			$\rightarrow {}^3P_0$
c_p		$^3S_1$	$\rightarrow {}^3S_1$
d_p			$\rightarrow {}^3D_1$
e_p			$\rightarrow {}^1P_1$
f_p			$\rightarrow {}^3P_1$
a_n	$n\Lambda \rightarrow nn$	$^1S_0$	$\rightarrow {}^1S_0$
b_n			$\rightarrow {}^3P_0$
f_n		$^3S_1$	$\rightarrow {}^3P_1$

where M are the masses and B are the binding energies.

In this chapter, we calculate these decay rates for the light s-shell hypernuclei: $^5_\Lambda$He, $^4_\Lambda$He and $^4_\Lambda$H, and study the non-mesonic decays of these hypernuclei. We use the transition potentials studied in the previous chapter and conventional wave functions [37, 38].

The wave function of the final N-N system is assumed to be the plane wave function for the moment,

$$\Psi_{NN}(\boldsymbol{r}, \boldsymbol{R}; \boldsymbol{k}, \boldsymbol{K}) = e^{i\boldsymbol{k}\cdot\boldsymbol{r}} e^{i\boldsymbol{K}\cdot\boldsymbol{R}} . \tag{3.4}$$

For initial Λ-N system, we construct the wave function in a shell model $i.e.$ by multiplying a wave function for Λ in hypernuclei and that for nucleon,

$$\Psi_{\Lambda N}(\boldsymbol{r}_\Lambda, \boldsymbol{r}_N) = \Psi_N(\boldsymbol{r}_N) \times \Psi_\Lambda(\boldsymbol{r}_\Lambda) . \tag{3.5}$$

We employ a Gaussian function for $\Psi_N(\boldsymbol{r}_N)$ for simplicity. On the other hand, we derive $\Psi_\Lambda(\boldsymbol{r}_\Lambda)$ from the wave function of light hypernuclei which is calculated in a so-called two-cluster model and given in the next section.

3.2 Wave functions of light hypernuclei

We calculate the wave functions of light hypernuclei in the so called two-cluster model, which represents a light hypernucleus by two parts: the Λ hyperon and the residual nucleus labeled by x. For example, x is a four nucleon system like an α particle for $^5_\Lambda$He. We solve the Schrödinger equation for the relative motion of the Λ hyperon and x. We denote the wave function by $\Psi(\boldsymbol{r})$, with $\boldsymbol{r}$, relative coordinate of two clusters.

The wave function $\Psi(\boldsymbol{r})$ can be obtained in the generator coordinate method (GCM). The spin of hypernuclei, $\boldsymbol{S}$, is the sum of total angular momentum of cluster x, $\boldsymbol{J_x}$, and spin of Λ, $\boldsymbol{S_\Lambda}$. The wave function for the state which have orbital angular momentum l and spin S is expressed by

$$\Psi(\boldsymbol{r}) = \sum_d f_{lj}(d)|\Phi(l;d), S; j\rangle . \tag{3.6}$$

where $\boldsymbol{j} = \boldsymbol{l} + \boldsymbol{S}$. Here $f_{lj}(d)$ are the GCM amplitudes and $\Phi(l;d)$ are the GCM basis wave function which is given by

$$\Phi(l;d) = \phi_l(r;d)Y_l(\hat{\boldsymbol{r}}) \tag{3.7}$$

$$\phi_l(r;d) = 4\pi(\sqrt{\pi}b_{\Lambda x})^{-3/2})\exp[\frac{-(r^2+d^2)}{2b_{\Lambda x}}]\mathcal{J}_l(\frac{rd}{b_{\Lambda x}^2}) \tag{3.8}$$

$$b_{\Lambda x} = \sqrt{\frac{(M_\Lambda + xM_N)}{xM_\Lambda}}b_N \tag{3.9}$$

where x stands the number of nucleon in x cluster. The generator coordinate d in the wave packet $\phi_l(r;d)$ specifies the distance between two clusters. The $\mathcal{J}_l$ is the l-th order spherical Bessel function with an imaginary argument. The GCM amplitudes f_{lj} are given by the solution of the GCM equation

$$\sum_{d_2}[H_{lj}(d_1, d_2) - EN_{lj}(d_1, d_2)] f_{lj}(d_2) = 0 \tag{3.10}$$

where the energy and normalization kernel are defined by

$$H_{lj}(d_1, d_2) = \langle\Phi(l;d_1), S; j| H |\Phi(l;d_2), S; j\rangle \tag{3.11}$$

$$N_{lj}(d_1, d_2) = \langle\Phi(l;d_1), S; j| 1 |\Phi(l;d_2), S; j\rangle \tag{3.12}$$

where H is the Hamiltonian of the Λ-x system.
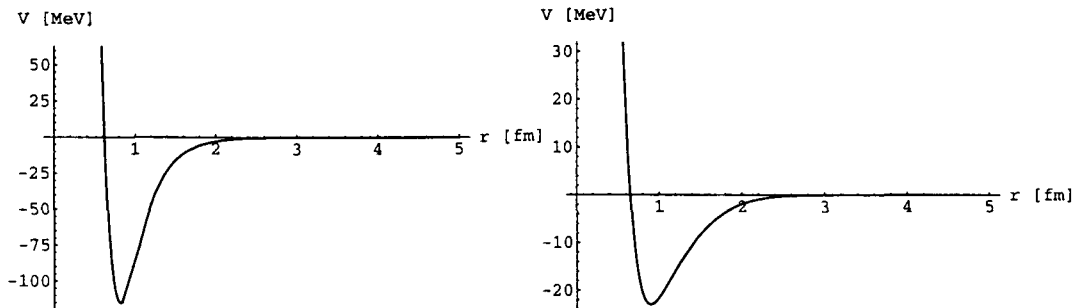
Figure 3.1: YNG potential for even l state(left) and odd l state(right).

The Hamiltonian H of the Λ-x system is given by the sum of the kinetic energy T and a potential energy $V_{\Lambda x}$

$$H = T + V_{\Lambda x} \ . \tag{3.13}$$

The potential energy $V_{\Lambda x}$ is obtained by folding the potential energy between Λ and nucleon. In the present study, we construct it by folding the YNG potential with $(0S)^x$ for the internal wave function of the x cluster. We employ YNG potential given in ref. [24], which is based on Nijmegen model D and the k_f is fixed 0.9 fm^{-1} for light hypernuclei. The spin averaged YNG potentials are shown in Fig 3.1.

For hypernucleus $^5_\Lambda$He, we take Gaussian parameter b_N for $0S$ as 1.358 fm [37, 38]. We present the folding potential from even l state in Fig 3.2. Using this potential energy, we solve the GCM equation eq.(3.10) with seven mesh points for the Λ-x distance parameter

$$d = 0.0, 1.0, 2.5, 4.0, 5.5, 7.0 \text{ and } 8.0 \text{ fm}. \tag{3.14}$$

We obtain the following ground state energy and the corresponding GCM amplitudes.

$$E = -3.08 \text{MeV} \tag{3.15}$$

$$f = (0.844, -0.415, 0.217, -0.181, 0.123, \cdots) \tag{3.16}$$

Fig 3.3 shows the obtained wave function $\Psi(r)$. This wave function is considerably different from the one which is obtained with one range Gaussian (ORG) ΛN interaction. As shown

41

in Fig 3.2, the potential energy $V_{\Lambda x}$ is repulsive at the short distance, reflecting the presence of the repulsive soft core in the YNG interaction. Therefore the obtained wave function is pushed away to the outside as compared with ORG correspondent. This feature gives rise to a sizable difference between the r.m.s. estimates of the α-Λ distance, 3.06 fm in YNG while 2.69 fm in ORG. The confirmation of this Λ wave function is difficult. Motoba *et al.* applied this wave function to the pionic decay of $^5_\Lambda$He and found that the YNG one is more reasonable than ORG one [39].

The wave function $\Psi(r)$ for $^4_\Lambda$He or $^4_\Lambda$He is calculated in the same way. In the 4-body case, the Gaussian parameter b_N for $0S$ is taken as 1.65 fm [37, 38].

These wave functions are used as $\Psi_\Lambda(r_\Lambda)$ in eq.(3.5), the wave function of Λ.

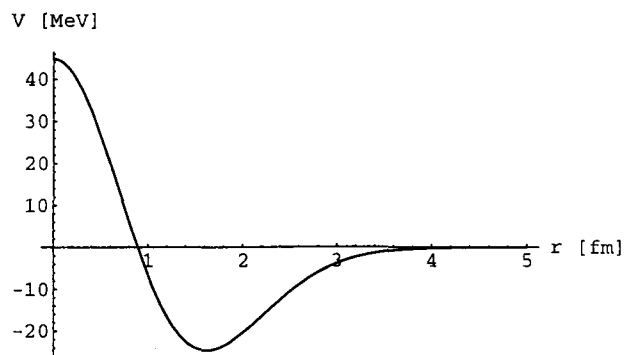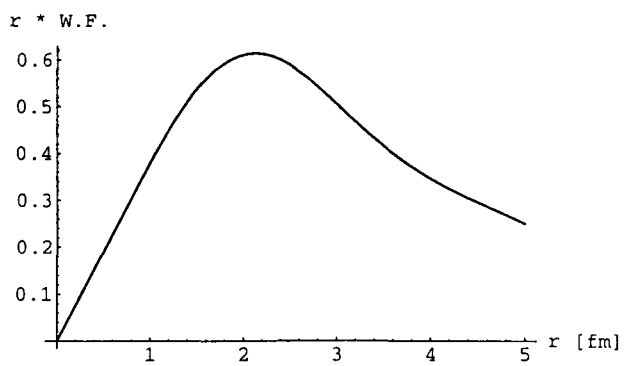Figure 3.2: Folded potential for $^5_\Lambda$He for even l state.

Figure 3.3: Wave function for Λ-α system.

3.3   Calculation

In computing the matrix element in eq.(3.2), we first perform the the Moshinsky transform for the two-baryon ΛN wave function $\Psi_{\Lambda N}(r_\Lambda, r_N)$ in order to separate the relative motion and the center of mass motion. The resulting wave function can be expressed as

$$\Psi_{\Lambda N}(r, R) = \sum_{nN} W_{nN} u_{n0}(r, b_r) Y_{00}(\hat{r}) u_{N0}(R, b_R) Y_{00}(\hat{R}) . \tag{3.17}$$

Here for the 4-body case, $b_r = 2.24$ fm, $b_R = 1.61$ fm and

$$W_{nN} = \begin{pmatrix} 0.8879 & -0.1196 & 0.02795 & \cdots \\ -0.2109 & 0.0899 & -0.03696 & \cdots \\ 0.0868 & -0.0651 & 0.02779 & \cdots \\ \vdots & \vdots & \vdots & \ddots \end{pmatrix}, \tag{3.18}$$

while for the 5-body case, $b_r = 1.84$ fm, $b_R = 1.21$ fm and

$$W_{nN} = \begin{pmatrix} 0.8523 & -0.1635 & 0.03598 & \cdots \\ -0.2379 & 0.0959 & -0.04612 & \cdots \\ 0.0762 & -0.0671 & 0.03534 & \cdots \\ \vdots & \vdots & \vdots & \ddots \end{pmatrix}. \tag{3.19}$$

In evaluating the two body matrix elements in the shell model wave function, one has to consider the effect of the short-range correlation between two baryons. For evaluating the amplitude of the OPE potential, we use a short range correlation which is obtained in the Nijmegen model D [37, 38]. However, Nijmegen model D has a hard core at short distance, which seems inconsistent with the constituent quark picture. Therefore, we use the following form of the short range correlation in evaluating the matrix element of the DQ potential.

$$u_{n0}(r, b_r) \quad \rightarrow \quad \frac{1}{N} u_{n0}(r, b_r) \left(1 - C_i Exp[-\frac{r^2}{r_i^2}] \right) \tag{3.20}$$

$$j_l(kr) \quad \rightarrow \quad j_l(kr) \left(1 - C_f Exp[-\frac{r^2}{r_f^2}] \right) \tag{3.21}$$

Here, C_i, C_f, r_i and r_f are parameters, and N is a normalization factor.

The direct quark induced transition potential depends on two quark model parameters that are the constituent quark mass m and the Gaussian parameter b. We use $m = 313$ MeV and $b = 0.5$ fm in the present calculation.

44

The OPE potential given in Table 2.1 does not contain the momentum dependence at the vertices. Therefore we take the following form factor into account

$$f(r) \quad \rightarrow \quad f(r) - \left(\frac{\Lambda_\pi}{\tilde{m}_\pi}\right)^3 f(\Lambda_\pi r) \tag{3.22}$$

$$f(r)V(r) \quad \rightarrow \quad f(r)V(r) - \left(\frac{\Lambda_\pi}{\tilde{m}_\pi}\right)^3 f(\Lambda_\pi r)V(\Lambda_\pi r) \tag{3.23}$$

$$f(r)T(r) \quad \rightarrow \quad f(r)T(r) - \left(\frac{\Lambda_\pi}{\tilde{m}_\pi}\right)^3 f(\Lambda_\pi r)T(\Lambda_\pi r) \tag{3.24}$$

where $\Lambda_\pi^2 = 20\tilde{m}_\pi^2$ [25].

3.4 Results

In this section we present our results.

3.4.1 $^5_\Lambda$He

In this subsection, we present our results for the decay of $^5_\Lambda$He.

In $^5_\Lambda$He, there are two Λp bonds and two Λn bonds. The Λp or Λn system takes both spin S=0 and spin S=1 state. Thus spin average factor becomes 1/4 (3/4) for $S = 0$ ($S = 1$) channels. The total nonmesonic decay rate of $^5_\Lambda$He is given by

$$\Gamma_{nm}(^5_\Lambda\text{He}) = \Gamma^p_a + \Gamma^p_b + \Gamma^p_c + \Gamma^p_d + \Gamma^p_e + \Gamma^p_f + \Gamma^n_a + \Gamma^n_b + \Gamma^n_f \qquad (3.25)$$

where $\Gamma^p_a \sim \Gamma^f_n$ are the partial decay rates and calculated by

$$\Gamma^p_{a,b} = 2\frac{1}{4}\int \frac{d^3k}{(2\pi)^3}\int \frac{d^3K}{(2\pi)^3}(2\pi)\delta(E.C.)\left|\langle \Psi_{N^3}\Psi_{NN}|V^p_{a,b}|\Psi_{N^3}\Psi_{\Lambda N}\rangle\right|^2 \qquad (3.26)$$

$$\Gamma^p_{c,d,e,f} = 2\frac{3}{4}\int \frac{d^3k}{(2\pi)^3}\int \frac{d^3K}{(2\pi)^3}(2\pi)\delta(E.C.)\left|\langle \Psi_{N^3}\Psi_{NN}|V^p_{c,d,e,f}|\Psi_{N^3}\Psi_{\Lambda N}\rangle\right|^2 \qquad (3.27)$$

$$\Gamma^n_{a,b} = 2\frac{1}{4}\int \frac{d^3k}{(2\pi)^3}\int \frac{d^3K}{(2\pi)^3}(2\pi)\delta(E.C.)\left|\langle \Psi_{N^3}\Psi_{NN}|V^n_{a,b}|\Psi_{N^3}\Psi_{\Lambda N}\rangle\right|^2 \qquad (3.28)$$

$$\Gamma^n_f = 2\frac{3}{4}\int \frac{d^3k}{(2\pi)^3}\int \frac{d^3K}{(2\pi)^3}(2\pi)\delta(E.C.)\left|\langle \Psi_{N^3}\Psi_{NN}|V^n_f|\Psi_{N^3}\Psi_{\Lambda N}\rangle\right|^2 . \qquad (3.29)$$

First we study about the one pion exchange mechanism. Table 3.2 shows the partial decay rates obtained when we employ the one pion exchange induced potential. All the decay rates are written in the unit of Γ_Λ, the free Λ decay rate. We list three sets of results. The values listed under "no FF no Corr" are the result when we do not take the form factor and the short range correlation into account. The values listed under "with FF no Corr" are the result when we take only the form factor into account. The values listed under "with FF with Corr" are the result when we take both the form factor and the short range correlation into account. Because $\Delta I = 1/2$ is assumed for the weak $\Lambda N\pi$ vertex, these partial decay rates satisfy the relation $a_n/a_p = b_n/b_p = f_n/f_p = 2$.

In the "no Corr" case, the channel d_p is dominant. This comes from the tensor part of the transition potential and is enhanced due to a large momentum in the final state. One can see that the form factor reduces most partial decay rates much. In the " with FF with

Table 3.2: Calculated partial decay rates of $^5_\Lambda$He in the one pion exchange mechanism

Ch	no FF no Corr	with FF no Corr	with FF with Corr
a_p	0.0004	0.0101	0.0002
b_p	0.0126	0.0060	0.0031
c_p	0.0013	0.0303	0.1022
d_p	0.3918	0.1789	0.0415
e_p	0.1132	0.0544	0.0346
f_p	0.0251	0.0121	0.0093
a_n	0.0009	0.0202	0.0003
b_n	0.0251	0.0121	0.0063
f_n	0.0502	0.0242	0.0186

Corr" case, the channel c_p becomes large and is dominant. This comes from also the tensor part of the transition potential. In the "with FF with Corr" case, the final state of channel c_p contain D wave as well as S wave because of the tensor force in the residual interaction. In the OPE mechanism, the channel e_p has also large rate, while rate of channel a and b are very small.

Table 3.3 show calculated results and experimental data for the nonmesonic decay of $^5_\Lambda$He. We list the proton induced decay rate (Γ_p), the neutron induced decay rate (Γ_n), the total decay rate ($\Gamma_{tot} = \Gamma_p + \Gamma_n$), and the n-p ratio ($R_{np} = \Gamma_n/\Gamma_p$). One can see that the calculated Γ_p is in good agreement to experiment, while the calculated Γ_n is much smaller than experiment. The Γ_p is dominated by large contribution of the channels c and d which vanish in the neutron induced mode. Calculated n-p ratio is much smaller than the experimental one.

We turn to the direct quark mechanism. Table 3.4 shows the partial decay rate when we employ the direct quark induced potential. We list four sets of result which are calculated with different short range correlations. The conditions $r_i = r_f$ and $C_i = C_f$ are used for simplicity. The parameter r_0 is fixed as 0.5 fm which is equal to the Gaussian parameter b in the quark model. The partial decay rate for channel d_p is zero, because the direct quark

Table 3.3: Calculated nonmesonic decay of $^5_\Lambda$He in the one pion exchange mechanism.

	no FF no Corr	with FF no Corr	with FF with Corr	Exp
Γ_p	0.544	0.291	0.191	0.21 ± 0.07
Γ_n	0.076	0.056	0.025	0.20 ± 0.11
Γ_{nm}	0.621	0.348	0.216	0.41 ± 0.14
R_{np}	0.140	0.193	0.130	0.93 ± 0.55

potential has no $\Delta L = 2$ part. Most partial decay rates decrease as short range correlation strengths C_i or C_f increase. The reason must be that, due to the short range correlation, the wave functions are pushed outward and reduced at the inner region where the direct quark mechanism is important. These partial decay rates are comparable to the one pion exchange ones. It shows that the direct quark processes plays significant roles in nonmesonic decays of hypernuclei as we expect. This must be because of the large momentum transfer of the $\Lambda N \rightarrow NN$ process.

The property of the DQ mechanism is very different from the OPE one. In all the partial rates, the rate for c_p is largest. This is a similar to the OPE mechanism. In the proton channels, the rates of channel d and e are small which are large in the OPE mechanism. On the other hand, the channel e is large which is small in the OPE mechanism. In the neutron channels, the rate of channels a and f are large, while that of channel b is small.

Next we investigate the ΔI property of the direct quark mechanism. In the following, we employ $C_i = C_f = 0.5$. Table 3.5 shows the effects of the $\Delta I = 3/2$ part of the potential. The values listed under "with $\Delta I = 3/2$" are the results when we employ the full direct quark induced potential. While the values listed under "no $\Delta I = 3/2$" are the results when we omit the $\Delta I = 3/2$ part. One sees that the channels a and b, which are $J = 0$ transitions, get significant contribution from the $\Delta I = 3/2$ part. This result indicates that the $\Delta I = 1/2$ rule would be violated in the non-mesonic decays of light hypernuclei.

Table 3.3 shows the calculated results and the experimental data for the nonmesonic decay of $^5_\Lambda$He. The proton induced decay rate Γ_p in the DQ mechanism is smaller than that of OPE mechanisms. On the other hand, the neutron induced decay rate Γ_n in the DQ

Table 3.4: Calculated partial decay rates of $^5_\Lambda$He in the direct quark mechanism.

ch	$C_i = C_f = 0$	$C_i = C_f = 0.3$	$C_i = C_f = 0.5$	$C_i = C_f = 0.7$
a_p	0.0130	0.0150	0.0167	0.0185
b_p	0.0127	0.0120	0.0113	0.0105
c_p	0.0968	0.0690	0.0548	0.0440
d_p	0	0	0	0
e_p	0.0056	0.0061	0.0064	0.0067
f_p	0.0345	0.0353	0.0353	0.0352
a_n	0.0727	0.0516	0.0407	0.0322
b_n	0.0059	0.0066	0.0069	0.0073
f_n	0.0622	0.0642	0.0648	0.0650

Table 3.5: Calculated partial decay rates of $^5_\Lambda$He in the direct quark mechanism.

Ch	with $\Delta I = 3/2$	no $\Delta I = 3/2$
a_p	0.0167	0.0118
b_p	0.0113	0.0001
c_p	0.0548	0.0548
d_p	0	0
e_p	0.0064	0.0064
f_p	0.0353	0.0334
a_n	0.0407	0.0237
b_n	0.0069	0.0003
f_n	0.0648	0.0668

Table 3.6: Calculated nonmesonic decay of $^5_\Lambda$He in the direct quark mechanism.

	$C_i = C_f = 0$	$C_i = C_f = 0.3$	$C_i = C_f = 0.5$	$C_i = C_f = 0.7$	Exp
Γ_p	0.163	0.137	0.125	0.115	0.21 ± 0.07
Γ_n	0.141	0.122	0.112	0.104	0.20 ± 0.11
Γ_{nm}	0.304	0.260	0.237	0.219	0.41 ± 0.14
R_{np}	0.865	0.889	0.903	0.910	0.93 ± 0.55

mechanism is much larger than that of the OPE mechanism. This is due to large contribution of channel a_n and f_n. The total nonmesonic decay rate in the DQ mechanism is roughly equal to that of the OPE mechanism. The n-p ratio in the DQ mechanism is much lager than that of the OPE mechanism, and is about 0.9, which is close to the central value of the experimental data.

As we have argued in the previous chapter, the OPE mechanism and the DQ mechanism are independent each other. Therefore we may to superpose two potential induced by these two mechanisms. Because the relation between the phenomenological $\Lambda N\pi$ vertex in the OPE mechanism and the effective weak Hamiltonian $H_{eff}^{\Delta S=1}$ in the DQ mechanism is not known, the relative phase of the two potential cannot be determined. Thus we evaluate both the DQ $\pm$ OPE case. The results are listed in Table 3.7. One finds a large difference between the two choices of the relative phase, mostly in c_p and f_n. We find a good agreement to experiment in the OPE $-$ DQ combination.

Table 3.7: Calculated nonmesonic decay of $^{5}_{\Lambda}$He

Ch	OPE only	DQ only	OPE + DQ	OPE − DQ	Exp
a_p	0.0002	0.0167	0.0148	0.0188	
b_p	0.0031	0.0113	0.0026	0.0263	
c_p	0.1022	0.0548	0.2936	0.0204	
d_p	0.0415	0	0.0415	0.0415	
e_p	0.0346	0.0064	0.0113	0.0707	
f_p	0.0093	0.0353	0.0808	0.0085	
a_n	0.0003	0.0407	0.0343	0.0477	
b_n	0.0063	0.0069	0.00005	0.0263	
f_n	0.0185	0.0648	0.1525	0.0142	
Γ_p	0.191	0.125	0.445	0.186	0.21 ± 0.07
Γ_n	0.025	0.112	0.187	0.088	0.20 ± 0.11
Γ_{nm}	0.216	0.237	0.632	0.275	0.41 ± 0.14
R_{np}	0.132	0.903	0.420	0.474	0.93 ± 0.55

3.4.2 $^4_\Lambda$He

In this subsection, we present the results for decay of $^4_\Lambda$He.

In the $^4_\Lambda$He, there are two Λp bonds and one Λn bonds. The Λn pair is in the spin S=0 state so that the spin of $^4_\Lambda$He is equal to zero. Thus there is no channel f_n. The nonmesonic decay rate of $^4_\Lambda$He is given by

$$\Gamma_{nm}(^4_\Lambda He) = \Gamma^p_a + \Gamma^p_b + \Gamma^p_c + \Gamma^p_d + \Gamma^p_e + \Gamma^p_f + \Gamma^n_a + \Gamma^n_b \tag{3.30}$$

$$\tag{3.31}$$

where

$$\Gamma^p_{a,b} = 2\frac{1}{4}\int\frac{d^3k}{(2\pi)^3}\int\frac{d^3K}{(2\pi)^3}(2\pi)\delta(E.C.)\left|\langle\Psi_{N^2}\Psi_{NN}|V^p_{a,b}|\Psi_{N^2}\Psi_{\Lambda N}\rangle\right|^2 \tag{3.32}$$

$$\Gamma^p_{c,d,e,f} = 2\frac{3}{4}\int\frac{d^3k}{(2\pi)^3}\int\frac{d^3K}{(2\pi)^3}(2\pi)\delta(E.C.)\left|\langle\Psi_{N^2}\Psi_{NN}|V^p_{c,d,e,f}|\Psi_{N^2}\Psi_{\Lambda N}\rangle\right|^2 \tag{3.33}$$

$$\Gamma^n_{a,b} = \int\frac{d^3k}{(2\pi)^3}\int\frac{d^3K}{(2\pi)^3}(2\pi)\delta(E.C.)\left|\langle\Psi_{N^2}\Psi_{NN}|V^n_{a,b}|\Psi_{N^2}\Psi_{\Lambda N}\rangle\right|^2 . \tag{3.34}$$

Table 3.8 shows our results and experimental data. The result of the OPE mechanism is qualitatively same to $^5_\Lambda$He case. All the rates are reduced to about 80 %. On the other hand, the results in the DQ mechanism have qualitative differences. The rates of channel c_p and a_n are very small which are large in the $^5_\Lambda$He case. It shows that the DQ contribution is sensitive to the wave function of the initial ΛN system. In the results of combined calculation, one finds a large difference between the two choices in e_p, f_n and b_n. Both choices provide a good agreement to the experimental data. It seems that the OPE + DQ combination provides a better agreement, while the OPE − DQ combination is preferred in the $^5_\Lambda$He case.

Table 3.8: Calculated nonmesonic decay of $^4_\Lambda$He

	OPE only	DQ only	OPE+DQ	OPE−DQ	Exp
a_p	0.0001	0.0183	0.0154	0.0214	
b_p	0.0021	0.0087	0.0023	0.0192	
c_p	0.0818	0.0004	0.0922	0.0721	
d_p	0.0321	0	0.0321	0.0321	
e_p	0.0224	0.0048	0.0065	0.0478	
f_p	0.0065	0.0275	0.0607	0.0073	
a_n	0.0005	0.0013	0.0003	0.0033	
b_n	0.0083	0.0108	0.0002	0.0380	
f_n	0	0	0	0	
Γ_p	0.145	0.060	0.209	0.200	0.16 ± 0.02
Γ_n	0.009	0.012	0.0005	0.041	0.01 ± 0.05
Γ_{nm}	0.154	0.072	0.210	0.241	0.17 ± 0.04
R_{np}	0.061	0.202	0.002	0.206	$0.00 \sim 0.40$

3.4.3 $^4_\Lambda$H

In $^4_\Lambda$H, there are one Λp bond and two Λn bonds. The Λp pair is in the spin S=0 state so that the spin of $^4_\Lambda$He is equal to zero. Thus there are no channels c_p though f_p The nonmesonic decay rate of $^4_\Lambda$H is given by

$$\Gamma_{nm}(^4_\Lambda H) = \Gamma^p_a + \Gamma^p_b + \Gamma^n_a + \Gamma^n_b + \Gamma^n_f \tag{3.35}$$

where

$$\Gamma^p_{a,b} = \int \frac{d^3k}{(2\pi)^3} \int \frac{d^3K}{(2\pi)^3} (2\pi)\delta(E.C.) \left| \langle \Psi_{N^2} \Psi_{NN} | V^p_{a,b} | \Psi_{N^2} \Psi_{\Lambda N} \rangle \right|^2 \tag{3.36}$$

$$\Gamma^n_{a,b} = 2\frac{1}{4} \int \frac{d^3k}{(2\pi)^3} \int \frac{d^3K}{(2\pi)^3} (2\pi)\delta(E.C.) \left| \langle \Psi_{N^2} \Psi_{NN} | V^n_{a,b} | \Psi_{N^2} \Psi_{\Lambda N} \rangle \right|^2 \tag{3.37}$$

$$\Gamma^n_f = 2\frac{3}{4} \int \frac{d^3k}{(2\pi)^3} \int \frac{d^3K}{(2\pi)^3} (2\pi)\delta(E.C.) \left| \langle \Psi_{N^2} \Psi_{NN} | V^n_f | \Psi_{N^2} \Psi_{\Lambda N} \rangle \right|^2 . \tag{3.38}$$

Table 3.9 shows our result and experimental data. In our model, each partial decay rate is same as that of $^4_\Lambda$He except for a number of bonds and the spin average factor. At present, the experimental data are very limited, only the total nonmesonic decay rate is known. We have two predictions of the nonmesonic decay of $^4_\Lambda$He, OPE+DQ and OPE−DQ. Both choices reproduce the total decay rate, while they are different in details. In the OPE+DQ choice, the neutron induced decay is dominant, on the other hand, in the OPE−DQ choice, proton induced decay is much lager than the neutron one. It is clearly shown in n-p ratio R_{np}. According to our study of $^5_\Lambda$He and $^4_\Lambda$He, we prefer the OPE−DQ choice. If our approach is reasonable, the n-p ratio of $^4_\Lambda$H would be small.

We anticipate better detailed experimental data for the nonmesonic decay of $^4_\Lambda$He.

54

Table 3.9: Calculated nonmesonic decay of $^4_\Lambda$H

	OPE only	DQ only	OPE+DQ	OPE−DQ	Exp
a_p	0.0003	0.0366	0.0308	0.0428	
b_p	0.0041	0.0174	0.0046	0.0384	
c_p	0	0	0	0	
d_p	0	0	0	0	
e_p	0	0	0	0	
f_p	0	0	0	0	
a_n	0.0003	0.0006	0.0001	0.0017	
b_n	0.0041	0.0054	0.0001	0.0190	
f_n	0.0130	0.0504	0.1146	0.0124	
Γ_p	0.004	0.054	0.035	0.081	
Γ_n	0.017	0.057	0.115	0.033	
Γ_{nm}	0.022	0.110	0.150	0.114	0.17 ± 0.11
R_{np}	3.952	1.048	3.246	0.406	

3.5   Discussion and conclusion

Here we discuss about our results presented in previous sections.

It is shown that the one pion exchange mechanism is significant to the nonmesonic decay of light S shell hypernuclei but is not able to reproduce some of the experimental data. Our result shows that the direct quark processes in $\Lambda N \rightarrow NN$ are very significant to the decay. This mechanism provides as large contribution as the one pion exchange mechanism. Our results also show the direct quark mechanism is qualitatively different from the one pion exchange mechanism. There are channels where the one pion exchange mechanism has small contribution, while the direct quark mechanism dominates the transition. It is also shown that the direct quark mechanism causes a large $\Delta I = 3/2$ transition in several channels. Our results are qualitatively consistent with those of Maltman and Shmatikov [32], although the calculated amplitudes have quantitative differences.

The large $\Delta I = 3/2$ transition is very interesting. But one may wonder whether the present quark model with Hamiltonian $H_{eff}^{\Delta S=1}$ is capable to reproduce the $\Delta I = 1/2$ dominance of the free hyperon decay. We suggest that the answer is yes. When we study the free Λ decay in this approach, we did not find such a large $\Delta I = 3/2$ transition. We found the dominance of quark diagrams with internal weak vertex in which $\Delta I = 3/2$ amplitude vanish. It is known that the quark diagrams with internal weak vertex in the pionic decay of ground state baryons, $\Delta I = 3/2$ vertex vanishes because of the color symmetry of the quark model wave function. We did not find such a large $\Delta I = 3/2$ transition when we study the direct quark processes in the $\Sigma N \rightarrow NN$ transition. The large $\Delta I = 3/2$ transition is special for $\Lambda N \rightarrow NN$ transition. We insist that the $\Delta I = 1/2$ rule is violated in the $\Lambda N \rightarrow NN$ transition and nonmesonic decays of hypernuclei. When it is confirmed, it may be the first clear evidence for the $\Delta I = 3/2$ weak transition, which is expected in the standard theory of the weak interaction. In order to confirm this, more detailed experimental data are needed.

About the nonmesonic decay of $^5_\Lambda$He, our results show that the interference of OPE and DQ is large and that the decay is reproduced if we take the OPE−DQ combination. At present, we cannot say which phase is correct. Suppose the OPE−DQ combination is correct, about a half of Γ_p comes from the channel f and about a half of Γ_n comes from the

channel a, in our approach. At present, we cannot check this because there is no data for the partial decay rates. We hope that it is confirmed with new experimental data in a new future.

Our results for the nonmesonic decay of $^4_\Lambda$He show that the decay is reproduced in our approach. In the $^4_\Lambda$He case, both the combinations give similar results, $i.e.$ the interference effect is not so large. In the both combination, about a half of Γ_p come from the channel c, while Γ_n is dominated by the channel b in the OPE−DQ combination.

The nonmesonic decay of $^4_\Lambda$H is related to that of $^4_\Lambda$He in our model. In $^4_\Lambda$H case, the effect of interference term is large in the channel f_n, which does not contribute in the $^4_\Lambda$He decay. Suppose the OPE−DQ combination is correct, we have small n-p ratio. We hope that our results are confirmed in experiment in near future.

In the following, we over view the other mechanisms for the $\Lambda N \rightarrow NN$ transition.

First, we discuss the effect of the exchanging a heavy meson. Ramos et $al.$ (ref. [40]) describes the $\Lambda N \rightarrow NN$ transition in a full one-boson-exchange mechanism. The author includes not only the long-ranged pion but also the other pseudosclar mesons, η and K, as well as the vector mesons, ρ, ω and K^*. In constructing the transition potential induced by exchange of heavy mesons, the Nijemegen or the Jülich strong vertices $H_{NN\eta}, H_{NNK}, H_{N\rho}, H_{NN\omega}$ and H_{NNK^*} are employed. On the other hand, the weak vertices $H_{\Lambda N\eta}, H_{\Lambda NK}, H_{\Lambda N\rho}, H_{\Lambda N\omega}$ and $H_{\Lambda NK^*}$, which cannot be derived from hyperon-decay experiment, are determined using $SU(6)$ symetry and the soft meson theorem for the PV vertices and pole model for the PC vertices [41]. The nonmesonic weak decay of $^{13}_\Lambda C$ is studied in a shell model framework. The result shows that combined $\pi + \rho$ exchange mechanism predicts a very similar total decay rate to the OPE one. It is found that the total rate is reduced by more than 40% when K exchange is added. It is also found that K^* exchange compensate the K exchange and the total rate in combined $\pi + \rho + K + K^*$ is 10 % smaller than the OPE one. The contribution of η and ω are very small and tend to cancel with each other. Therefore the total rate in combined $\pi + \rho + K + K^* + \eta + \omega$ is similar to the OPE one. The addition of K exchange greatly reduces the n-p ratio while addition of other mesons does not change the result much. The final ratio is smaller than that of OPE and greatly underestimates the central value of experimental data.

Shmatikov studied the 2π exchange contribution. It is indicated that the diagrams with ΣN and NN intermediate states cancel with each other and the net effect contributes only to the $J = 0$ amplitudes [42].

Recently, Itonaga et $al.$ studied the σ meson exchange [38]. The coupling to the two pions are introduced instead of $H_{\Lambda N \sigma}$ weak vertex. For the nonmesonic weak decays of light s-shell hypernuclei and and $^{13}_{\Lambda}C$, it is found that the n-p ratios are improved by the σ-meson but are still far from the experimental data.

In all, the meson exchange contributions other than OPE seem to be small. Therefore describing the $\Lambda N \rightarrow NN$ transition by the OPE and DQ, seems to be reasonable.

Chapter 4

Summary

We study the nonmesonic decays of hypernuclei which represent to us a new type of the nonleptonic weak process, $\Lambda N \to NN$. The $\Lambda N \to NN$ transition has large momentum transfer due to the mass difference of Λ and N. The large momentum transfer makes the transition sensitive to the short distance quark structure of the two baryon system. We propose a new mechanism, direct quark mechanism, for this transition, which corresponds to direct quark process. We have derived the $\Lambda N \to NN$ transition potential induced by direct quark mechanism. We have employed an effective weak Hamiltonian for constituent quarks, which takes account of the one-loop perturbative QCD corrections. Then we have evaluated the transition matrix element to the first order in the weak interaction using the quark model wave functions of baryons. The flavor/spin structure of the potential reflects the SU(6) symmetry of the baryon wave functions, which have been verified in the low energy baryon spectrum and properties of the baryons.

In order to apply the obtained potential to the weak nonmesonic decays of the s-shell hypernuclei, hypernuclear wave function is calculated in the cluster model with the YNG interaction. The YNG interaction is an effective interaction between the hyperon and the nucleon which are placed in nuclei. The obtained wave functions are reasonable one which have been tested in many applications.

We apply the direct quark induced transition potential as well as the one pion exchange mechanism to the weak nonmesonic decays of s-shell hypernuclei. Our results show that the contribution of the direct quark processes is as large as that of the conventional one

pion exchange mechanism. The partial decay rates show distinctive features when they are compared to the one-pion exchange. Especially, the ratio of the neutron-induced and the proton-induced decay rates is discriminative of these mechanisms. Furthermore, we have found that the $J = 0$ transition channel has a large $\Delta I = 3/2$ contribution and therefore that the $\Delta I = 1/2$ rule is significantly broken. This may be the first clear evidence for the $\Delta I = 3/2$ weak transition, that is expected in the standard theory of the weak interaction.

We reproduce the nonmesonic decays of $^5_\Lambda$He and $^4_\Lambda$He in our approach where we superpose one pion exchange mechanism and direct quark one. We provide a prediction for the nonmesonic decays of $^4_\Lambda$He, to which experimental data are very limited. It is suggested that the ratios of the partial rates with various spin-isospin specification are useful in testing different mechanisms of the transition. Further experimental studies are most desirable.

There are a number of remaining problems. The relation between one pion exchange mechanism and direct quark mechanism is to be studied. The relation between phenomenological $\Lambda \to N\pi$ vertex and the effective weak Hamiltonian is not known. It is favorable to apply the same effective weak Hamiltonian to the mesonic decay as well so that a unified view of the hypernuclear decay is obtained. The $\Delta I = 1/2$ enhancement mechanism for the mesonic decay is especially important in this regard.

We have not considered so far the second order process with a $\Sigma - N$ intermediate state induced by a strong pion (meson) and/or quark exchanges. The short range part of potential for a weak $\Sigma N \to NN$ transition can be also computed in the same direct quark mechanism. It is found that the mixing of this potential does not change the main feature of present direct quark potential, though its contribution is not negligible quantitatively [35].

For hypernuclei other than the s-shell systems, we need a realistic calculation combined with the nuclear structure analysis. We have provided the baryonic two-body transition potential so that it can be used in any hypernuclear calculations. Futher study is needed.

Acknowledgements

Appendix A

Nuclear matter calculation

Momentum of Initial Λ and N

$$p_\Lambda = (M_\Lambda, 0) \qquad p_N = (p_{N0}, \vec{p}_N) \tag{A.1}$$

Momentum of two out going nucleons

$$k_1 = (k_{10}, \vec{k}_1) \qquad k_2 = (k_{20}, \vec{k}_2) \tag{A.2}$$

relative and c.m. momentum

$$\vec{p} = \frac{M_\Lambda}{M_\Lambda + M_N}\vec{p}_N \equiv \mu\, \vec{p}_N \tag{A.3}$$

$$\vec{p}_{cmi} = \vec{p}_N \tag{A.4}$$

$$\vec{q} = \frac{1}{2}(\vec{k}_1 - \vec{k}_2) \tag{A.5}$$

$$\vec{p}_{cmf} = \vec{k}_1 + \vec{k}_2 \tag{A.6}$$

Decay rate in the nuclear matter

$$\Gamma = 2\int^{k_F}\frac{d^3\vec{p}_N}{(2\pi)^3}\int\frac{d^3\vec{k}_1}{(2\pi)^3}\int\frac{d^3\vec{k}_2}{(2\pi)^3}(2\pi)^4\delta(p_\Lambda + p_N - k_1 - k_2)$$

$$\frac{1}{4}\sum_{\substack{S_i,\mu_i \\ S_f,\mu_f}} |< \vec{q}, S_f, \mu_f|H|\vec{p}, S_i, \mu_i >|^2 \tag{A.7}$$

$$= 2\frac{1}{\mu^3}\int^{\mu k_F}\frac{d^3\vec{p}}{(2\pi)^3}\int\frac{d^3\vec{q}}{(2\pi)^3}\int\frac{d^3\vec{p}_{cmf}}{(2\pi)^3}(2\pi)^3\delta(\vec{p}_{cmi} - \vec{p}_{cmf})(2\pi)\delta(E.C.)$$

$$\frac{1}{4}\sum_{\substack{S_i,\mu_i \\ S_f,\mu_f}} |< \vec{q}, S_f, \mu_f|H|\vec{p}, S_i, \mu_i >|^2 \tag{A.8}$$

Table A.1: Calculated observables. All the decay rate is in the unit of Γ_{free}.

	Direct Quark		OPE
	Full	$\Delta I = 1/2$	
Γ	0.675	0.488	1.613
Γ_p	0.339	0.193	1.457
Γ_n	0.335	0.294	0.156
R_{np}	0.98	1.52	0.10
a_1	-0.29	-0.49	-0.18

$$= 2\frac{1}{\mu^3} \int^{\mu k_F} \frac{d^3\vec{p}}{(2\pi)^3} \int \frac{d^3\vec{q}}{(2\pi)^3} (2\pi)\delta(E.C.) \frac{1}{4} \sum_{\substack{S_i,\mu_i \\ S_f,\mu_f}} |< \vec{q}, S_f, \mu_f |H| \vec{p}, S_i, \mu_i >|^2 \qquad (A.9)$$

$$= 2\frac{1}{\mu^3} \int^{\mu k_F} \frac{p^2 dp}{(2\pi)^3} \int \frac{q^2 dq}{(2\pi)^3} (2\pi)\delta(E.C.) \int \hat{p} \int \hat{q} \frac{1}{4} \sum_{\substack{S_i,\mu_i \\ S_f,\mu_f}} |< \vec{q}, S_f, \mu_f |H| \vec{p}, S_i, \mu_i >|^2 (A.10)$$

Partial wave decomposition and $\hat{p}$ and $\hat{q}$ integration

$$\Gamma = 2\frac{1}{\mu^3} \int^{\mu k_F} \frac{p^2 dp}{(2\pi)^3} \int \frac{q^2 dq}{(2\pi)^3} (2\pi)\delta(E.C.)$$
$$\left\{ \frac{1}{4}a_p(p,q)^2 + \frac{1}{4}b_p(p,q)^2 + \frac{3}{4}c_p(p,q)^2 + \frac{3}{4}d_p(p,q)^2 + \frac{3}{4}e_p(p,q)^2 + \frac{3}{4}f_p(p,q)^2 \right.$$
$$\left. + \frac{1}{4}a_n(p,q)^2 + \frac{1}{4}b_n(p,q)^2 + \frac{3}{4}f_n(p,q)^2 \right\} \qquad (A.11)$$

Energy conservation rule and $\delta(E.C.)$

$$M_\Lambda + \frac{1}{2M_\Lambda}|\vec{p}|^2 M_N + \frac{1}{2M_N}|\vec{p}|^2 = 2M_N + 2\frac{1}{2M_N}|\vec{q}|^2 \qquad (A.12)$$

$$\delta(E.C.) = \delta\left(\frac{1}{M_N}|\vec{q}|^2 - M_\Lambda + M_N - \frac{1}{2\mu M_N}|\vec{p}|^2\right) \qquad (A.13)$$

$$q(p) \equiv \sqrt{M_N(M_\Lambda - M_N) + \frac{1}{2\mu}p^2} \qquad (A.14)$$

Final formula

$$\Gamma = 2\frac{1}{\mu^3} \int^{\mu k_F} \frac{p^2 dp}{(2\pi)^3} \frac{1}{(2\pi)^2} \frac{M_N}{2} q(p)$$
$$\left\{ \frac{1}{4}a_p(p,q(p))^2 + \frac{1}{4}b_p(p,q(p))^2 + \frac{3}{4}c_p(p,q(p))^2 + \frac{3}{4}d_p(p,q(p))^2 + \frac{3}{4}e_p(p,q(p))^2 \right.$$
$$\left. + \frac{3}{4}f_p(p,q(p))^2 + \frac{1}{4}a_n(p,q(p))^2 + \frac{1}{4}b_n(p,q(p))^2 + \frac{3}{4}f_n(p,q(p))^2 \right\} \qquad (A.15)$$

63

Appendix B

Our previous calculation

The decay of $^{5}_{\Lambda}\text{He}$

$$\Gamma\left(^{5}_{\Lambda}\text{He}\right) = 2\,\Gamma_{\Lambda p \to pn} + 2\,\Gamma_{\Lambda n \to nn}\ . \tag{B.1}$$

Spin averaged two-body transition rates, $\Gamma_{\Lambda p \to pn}$ and $\Gamma_{\Lambda n \to nn}$,

$$\Gamma = \frac{1}{4}\sum_{\substack{s_i,\mu_i \\ s_f,\mu_f}} \int \frac{d^3\vec{K}}{(2\pi)^3} 2\pi\delta(E.C.) \left| \int \frac{d^3\vec{p}}{(2\pi)^3} \int \frac{d^3\vec{q}}{(2\pi)^3} \psi_{fin}(\vec{q};\vec{K})\ V_{\substack{s_i,\mu_i \\ s_f,\mu_f}}(\vec{p},\vec{q})\ \psi_{ini}(\vec{p}) \right|^2\ . \tag{B.2}$$

Energy conservation rule and $\delta(E.C.)$

$$M_\Lambda + M_N = 2\frac{K^2}{2M_N} + 2M_N \tag{B.3}$$

$$\delta(E.C.) = \frac{M_N}{2K}\delta(K - K^*) \quad K^* = 415.9\text{MeV} \tag{B.4}$$

Partial waves decomposition and $\vec{K}$ integration

$$\Gamma = \frac{1}{(2\pi)^2}\frac{M_N K^*}{2}\frac{1}{4}\sum_{\substack{L_i,S_i,J,m \\ L_f,S_f,J,m}} \left| \int \frac{p^2 dp}{(2\pi)^3} \int \frac{q^2 dq}{(2\pi)^3} \psi^{fin}_{L_f}(q;K^*)\ V_{\substack{L_i,S_i,J \\ L_f,S_f,J}}(p,q)\ \psi^{ini}_{L_i}(p) \right|^2\ , \tag{B.5}$$

Spin averaged two-body transition rates,

$$\Gamma_{\Lambda p \to pn} = \frac{M_N K^*}{2(2\pi)^2}\frac{1}{4}(|a_p|^2 + |b_p|^2 + 3|c_p|^2 + 3|d_p|^2 + 3|e_p|^2 + 3|f_p|^2) \tag{B.6}$$

$$\Gamma_{\Lambda n \to nn} = \frac{M_N K^*}{2(2\pi)^2}\frac{1}{4}(|a_n|^2 + |b_n|^2 + 3|f_n|^2)\ . \tag{B.7}$$

Amplitudes

$$a_p \equiv \int \frac{p^2 dp}{(2\pi)^3} \int \frac{q^2 dq}{(2\pi)^3} \psi^{fin}_0(q;K^*)V^{proton}_a(p,q)\psi^{ini}_0(p) \tag{B.8}$$

Our simple wave functions for the initial and the final state

$$\psi_{ini}(\vec{R}) = N_\psi g(\vec{R}) \exp\left\{-\frac{1}{2B^2}\vec{R}^2\right\} \quad B = \sqrt{2} \times 1.3\text{fm} \tag{B.9}$$

$$\psi_{fin}(\vec{R}; \vec{K^*}) = g(\vec{R}) \exp\left\{i\vec{K^*}\cdot\vec{R}\right\} \quad K^* = 415.9\text{MeV} \tag{B.10}$$

g : short range correlation,

$$g(\vec{R}) = 1 - C\exp\left[-\frac{R^2}{r_0^2}\right] \quad C = 0.5 \ \ r_0 = 0.5\text{fm} \tag{B.11}$$

Two body transition rates Γ_{NS}

$$\Gamma_{p0} = \frac{M_N K^*}{2(2\pi)^2}(|a_p|^2 + |b_p|^2) \tag{B.12}$$

$$\Gamma_{p1} = \frac{M_N K^*}{2(2\pi)^2}(|c_p|^2 + |d_p|^2 + |e_p|^2 + |f_p|^2) \tag{B.13}$$

$$\Gamma_{n0} = \frac{M_N K^*}{2(2\pi)^2}(|a_n|^2 + |b_n|^2) \tag{B.14}$$

$$\Gamma_{n1} = \frac{M_N K^*}{2(2\pi)^2}|f_n|^2 \ . \tag{B.15}$$

$$\Gamma_{\Lambda p \to pn} = \frac{1}{4}(\Gamma_{p0} + 3\Gamma_{p1}) \ , \tag{B.16}$$

$$\Gamma_{\Lambda n \to nn} = \frac{1}{4}(\Gamma_{n0} + 3\Gamma_{n1}) \ , \tag{B.17}$$

n-p ratio

$$R_{np} \cong \frac{\Gamma_{\text{neutron induced}}}{\Gamma_{\text{proton induced}}} \ . \tag{B.18}$$

n-p ratio for the spin-average hypernuclei

$$R_{np} = \frac{\Gamma_{n0} + 3\Gamma_{n1}}{\Gamma_{p0} + 3\Gamma_{p1}} \ . \tag{B.19}$$

The angular distribution of the outgoing proton

$$W(\theta) = 1 + a_1(p)\, \mathcal{P}_\Lambda\, P_1(\cos\theta) \ . \tag{B.20}$$

Asymmetry parameter

$$a_1(^5_\Lambda\text{He}) = \frac{2\sqrt{3}\,(\sqrt{2}c_p + d_p)f}{a_p^2 + b_p^2 + 3(c_p^2 + d_p^2 + e_p^2 + f_p^2)} \ . \tag{B.21}$$

65

Other observables

$$R_{np}(^5_\Lambda He) = \frac{\Gamma_{n0} + 3\Gamma_{n1}}{\Gamma_{p0} + 3\Gamma_{p1}} \tag{B.22}$$

$$R_{np}(^4_\Lambda He) = \frac{2\Gamma_{n0}}{\Gamma_{p0} + 3\Gamma_{p1}} \tag{B.23}$$

$$\frac{\Gamma_{n.m.}(^4_\Lambda He)}{\Gamma_{n.m.}(^4_\Lambda H)} = \frac{\Gamma_{p0} + 3\Gamma_{p1} + 2\Gamma_{n0}}{2\Gamma_{p0} + \Gamma_{n0} + 3\Gamma_{n1}} \tag{B.24}$$

Table B.1: Calculated transition amplitudes in 10^{-10} MeV$^{-1/2}$.

	isospin	spin orbital	Direct Quark full	$\Delta I = 1/2$	$\Delta I = 3/2$	OPE
a_p	$p\Lambda \to pn$	$^1S_0 \to {}^1S_0$	-78.1	-23.4	-54.7	2.2
b_p		$\to {}^3P_0$	-53.5	2.0	-55.5	-24.8
c_p		$^3S_1 \to {}^3S_1$	-1.0	-1.0	0	2.2
d_p		$\to {}^3D_1$	0	0	0	-86.8
e_p		$\to {}^1P_1$	-23.2	-23.2	0	-43.0
f_p		$\to {}^3P_1$	-55.4	-53.8	-1.5	20.2
a_n	$n\Lambda \to nn$	$^1S_0 \to {}^1S_0$	5.5	-33.1	38.6	3.1
b_n		$\to {}^3P_0$	42.2	2.9	39.3	-35.1
f_n		$^3S_1 \to {}^3P_1$	-75.1	-76.2	1.0	28.6

Table B.2: Calculated observables. All the decay rates are in the unit of Γ_{free}.

	Direct Quark		OPE	DQ and OPE		Exp
	Full	$\Delta I = \frac{1}{2}$		DQ+OPE	DQ−OPE	
Γ_{p0}	0.177	0.010	0.012	0.235	0.143	$0 \sim 0.116$
Γ_{p1}	0.071	0.067	0.193	0.260	0.269	$0.074 \sim 0.187$
Γ_{n0}	0.035	0.021	0.024	0.002	0.118	$0.063 \sim 0.553$
Γ_{n1}	0.111	0.114	0.016	0.042	0.212	$0.049 \sim 0.196$
$\Gamma_{\Lambda p \to pn}$	0.097	0.053	0.143	0.253	0.238	0.105 ± 0.035
$\Gamma_{\Lambda n \to nn}$	0.092	0.091	0.018	0.032	0.189	0.100 ± 0.055
$\Gamma\left(^5_\Lambda\text{He}\right)$	0.378	0.295	0.333	0.573	0.854	0.41 ± 0.14
$R_{np}(^5_\Lambda\text{He})$	0.94	1.70	0.12	0.12	0.79	0.93 ± 0.55
$a_1(^5_\Lambda\text{He})$	0.01	0.02	−0.19	0.20	−0.44	(≤ -0.6)
$R_{np}(^4_\Lambda\text{He})$	0.18	0.20	0.08	0.004	0.24	0.18 ± 0.12
$\dfrac{\Gamma_{n.m.}(^4_\Lambda\text{He})}{\Gamma_{n.m.}(^4_\Lambda\text{H})}$	0.63	0.66	6.58	1.69	1.14	1.65 ± 0.77
Γ_{n0}/Γ_{p0}	0.20	2.00	2.00	0.01	0.854	$0 + 2.75$

Bibliography

[1] Particle Data Group Phys. Rev. **D50**(1994)1728

[2] L.B. Okun, *Leptons and Quarks* (North Holland, The Netherlands, 1982)

[3] A.I. Vainshtein, V.I. Zakharov and M.A. Shifman, Sov. Phys. JETP, 45(1977)670

[4] F. J. Gilman and M. B. Wise, Phys. Rev. **D20**(1979)2382

[5] E.A. Paschos, T. Schneider, and Y.L. Wu, Nucl. Phys. **B332**(1990)285

[6] M.M. Block and R.H. Dalitz, Phys. Rev. Lett. **11**(1963)96

[7] J.J. Szymanski *et al.* Phys. Rev. **C43**(1991)849

[8] V.J. Zeps, and G.B. Franklin for the E788 Collaboration
Proceedings of the 23rd INS International Symposium on
Nuclear and Particle Physics with Meson Beams in 1 GeV/c Region, P227

[9] R.A. Schumacher, Nucl. Phys. **A547**(1992)143c

[10] R.A. Schumacher for the E788 Collabolation
Proceedings of the U.S.-Japan Seminar on Properties & Interactions of Hyperons,
ed. by B. F. Gibson, P. D. Barnes and K. Nakai (World Scientific, 1994), P85

[11] T. Kishimoto,
Proceedings of the U.S.-Japan Seminar on Properties & Interactions of Hyperons,
ed. by B. F. Gibson, P. D. Barnes and K. Nakai (World Scientific, 1994), P101

[12] S. Ajimura et al. Phys. Lett. **B282**(1992)293

[13] W.A. Bardeen, A.J. Buras and J.M. Gerard Phys. Lett. **B192**(1987)138

[14] T. Morozumi, C.S. Lim and A.I. Sanda, Phys. Rev. Lett. **65**(1990)404

[15] M. Takizawa, T. Inoue, and M. Oka, Prog. Theor. Phys. Suppl. **120**(1995)335

[16] K.G. Wilson, T.S. Walhout, A. Harindranath, W.M. Zhang,
     R.J. Perry and St.D. Glazek, Phys. Rev. **D49**(1994)6720

[17] Y.Nambu and G.Jona-Lasinio, Phys. Rev. **122**(1961)345

[18] N. Isugur and G. Karl, Phys. Rev. **D18**(1978)4187

[19] M. Oka, K. Shimizu and K. Yazaki, Phys. Lett. **B130**(1983)365;
     Nucl. Phys. **A464**(1987)700; M. Oka, Phys. Rev. **D38**(1988)298.

[20] M. Oka and S. Takeuchi, Phys. Rev. Lett. **63**(1989)1780.

[21] M. Oka and K. Yazaki, Phys. Lett. **B90**(1980)41

[22] M. Oka and S. Takeuchi, Nucl. Phys. **A524**(1991)649;
     S. Takeuchi and M. Oka, Phys. Rev. Lett. **66**(1991)1271.

[23] M.M Nagels, T.A.Rijken and J.J. deSwart, Phys. Rev. **D12**(1975)744,
     Phys. Rev. **D15**(1977)2547, Phys. Rev. **D20**(1979)1633

[24] Y.Yamamoto and H.Bandō, Prog. Theor. Phys. **73**(1985)905,
     Prog. Theor. Phys. Suppl. **81**(1985)42, Prog. Theor. Phys. **83**(1990)254

[25] K. Takeuchi, H. Takaki and H. Bando, Prog. Theor. Phys. **73**(1985)841

[26] B.H.J. Mckellar and B.F. Gibson, Phys. Rev. **C30**(1984)322

[27] A. Ramos, E. van Meijgaard, C. Bennhold, and B. K. Jennings,
     Nucl. Phys. **A544**(1992)703

[28] Y. Abe *et al.*, Prog. Theor. Phys. **64**(1980)1363.

[29] J. Cohen, Prog. in Part. and Nucl. Phys. **25**(1990)139

[30] H. Bando, T. Motoba and J. Zofka, Int. Jour. Mod. Phys. **A5**(1990)4021

[31] C. Y. Cheung, D. P. Heddle and L. S. Kisslinger, Phys. Rev. **C27**(1983)335

[32] K. Maltman and M. Shmatikov, Phys. Lett. **B331**(1994)1

[33] M. Oka, T. Inoue and S. Takeuchi,
Proceedings of the U.S.-Japan Seminar on Properties & Interactions of Hyperons,
ed. by B. F. Gibson, P. D. Barnes and K. Nakai (World Scientific, 1994), P119

[34] T. Inoue, S. Takeuchi and M. Oka, Nucl. Phys. **A577**(1994)281c
Proceedings of the International Symposium on
SPIN-ISOSPIN RESPONSES AND WEAK PROCESSES IN HADRONS AND NUCLEI,
ed. by H.Ejiri, Y.Mizuno and T.Suzuki

[35] M. Oka, T. Inoue and S. Takeuchi,
Proceedings of the IV Internationnal Symposium on,
WEAK AND ELECTROMAGNETIC INTERACTIONS IN NUCLEI,
ed. by H. Ejiri, T. Kishimoto and T. Sato (World Scientific, 1995), P540

[36] T. Inoue, S. Takeuchi and M. Oka, Nucl. Phys. **A597**(1996)563

[37] Y. Yamamoto, T. Motoba, H. Himeno, K. Ikeda and S. Nagata,
Prog. Theor. Phys. Suppl. **117**(1994)361

[38] T. Motoba and K. Itonaga, Prog. Theor. Phys. Suppl. **117**(1994)477

[39] T. Motoba Nucl. Phys. **A547**(1992)115
Proceedings of the Internationnal Symposium on Hypernuclear and Strange Particle Physics,
ed. by T. Fukuda, O. Morimatsu,T. Yamazaki and K. Yazaki

[40] A. Ramos and C. Bennhold, Nucl. Phys. **A577**(1994)287c,
Proceedings of the International Symposium on
SPIN-ISOSPIN RESPONSES AND WEAK PROCESSES IN HADRONS AND NUCLEI,
ed. by H. Ejiri, Y. Mizuno and T. Suzuki,
A. Parreno, A. Ramos, and C.Bennhold, preprint

70

[41] J.F. Dubach, G.B. Feldman, B.R. Holstein and L. de la Torre, preprint

[42] M. Shmatikov, Preprint IAE-5708/2 M. 1994

[43] K. Itonaga, T. Ueda and T. Motoba, Nucl. Phys. **A577**(1994)301c

Proceedings of the International Symposium on

SPIN-ISOSPIN RESPONSES AND WEAK PROCESSES IN HADRONS AND NUCLEI,

ed. by H.Ejiri, Y.Mizuno and T.Suzuki

K. Itonaga, T. Ueda and T. Motoba, Nucl. Phys. **A585**(1995)331c

Proceedings of the International Conference on Hypernuclear and Strange Particle Physics,

ed. by C.A.Davis, H.W.Fearing and B.K.Jennings